# HEAVY SECTION AUSTENITIC STAINLESS STEEL FOR HEADERS AND PIPING IN HIGH-EFFICIENT BIOMASS-FIRED POWER PLANTS

RAPPORT 2023:930





# Heavy section austenitic stainless steel for the future header and piping material in high-efficient biomass-fired power plants

MATTIAS CALMUNGER, GUOCAI CHAI, MARIA SUNDQVIST, VESNA BARIŠIĆ, KYÖSTI VÄNSKÄ, BERTIL WAHLUND, MIKAEL SEGERSÄLL, JOHAN MOVERARE OCH HUGO WÄRNER

#### **Foreword**

The project has been performed within the framework of the materials technology research programme KME, Consortium materials technology for thermal energy processes, period 2018-2023. The consortium is at the forefront of developing material technology to create maximum efficiency for energy conversion of renewable fuels and waste.

KME was established 1997 and is a multi-cliental group of companies over the entire value chain, including stakeholders from the material producers, manufacturers of systems and components for energy conversion and energy industry (utilities), that are interested in materials technology research. The consortium is managed by Energiforsk.

The programme activities are characterised by long term industry and demand driven research, and contribute to the development of thermal energy processes for efficient utilisation of renewable fuels and waste in power and heat production. The KME goals are to bring about cost-effective materials solutions for increased availability and power production, improved fuel flexibility and improved operating flexibility, with low environmental impact.

The specific project has been analysing new candidate materials with improved creep and fatigue strength to meet increased steam data and numbers of start-and-stop cycles in boilers. Mattias Calmunger, LiU, has been the project leader. Mattias Calmunger, Mikael Segersäll, Johan Moverare and Hugo Wärner, LiU, Guocai Chai and Maria Sundqvist, Alleima, Vesna Barišić and Kyösti Vänskä, Sumitomo, and Bertil Wahlund, Energiforsk, have been project participants and co-authors of the report. The industry has participated in the project through own investment (60 %) and the Swedish Energy Agency has financed the academic partners (40 %).

Energiforsk would like to thank all the participants for a well performed project.

Bertil Wahlund, Energiforsk

These are the results and conclusions of a project, which is part of a research programme run by Energiforsk. The authors are responsible for the content.



## **Summary**

The project is a part of the industry initiative and forum KME. With increasing requirements on improved creep and fatigue strength, from increased steam data and numbers of start-and-stop cycles, the currently used ferritic steels in heavy section components of high-efficient biomass-fired power plants are not sufficient.

From previous studies, advanced heat resistant austenitic stainless steels (A-ASS) have showed to be promising candidates, with high reliability and more cost-effective compared to other candidate material such as nickel-based alloys. However, more investigations are needed to verify that heavy section A-ASS have sufficient safety and reliability compared to currently used materials, such as the ferritic steels P91 and P92. Mechanical behaviour such as creep, fatigue and thermo-mechanical fatigue (TMF) have been investigated on aged materials to simulate long-term use.

The candidate materials experienced a detrimental effect on the TMF performance by the influence of ageing. The reduction in TMF performance was attributed to an accelerated microstructural evolution that provided decreased effectiveness for impeding dislocation motion. Comparing TMF performance, Sanicro 25 showed compared to Esshete 1250 a better performance and higher strength for OP testing conditions including virgin and aged materials. This was attributed to the superior microstructural strengthening mechanisms during high temperature conditions. The two alloys exhibit different crack propagation and fatigue and creep behaviour, mainly due to the microstructural evolution during loading. Coherent copper precipitates and incoherent Nb-carbides acted as dislocation obstacles and therefore add to the prominent hardening effect and high temperature properties of Sanicro. Esshete 1250 solely experienced fracture along the grain boundaries. A fatigue and creep crack propagation process of Sanicro 25 was proposed, which involved dynamic recrystallization (DRX) of the crack tip plastic zone. The precipitation behaviour of the candidate materials as well as their impact on the deformation, damage and failure mechanisms have been evaluated in the project. However, due to the unsatisfactory welding results the toughness of welded and aged materials could not be evaluated.

Moreover, the project has showed that Sanicro 25 could be used to reduce the weight of the power plant components compared to currently used material and with maintained safety.

The project resulted in new knowledge and understanding of the two candidate austenitic stainless steels mechanical and microstructural evolution during TMF, fatigue and creep as well as structural stability in regards of precipitation. This new knowledge can be used as a base for material selection regarding the future use of these materials in heavy section components in biomass-fired power plants. In addition, the new knowledge and understanding can be used for material development and to some extent lighter power plant design.



## Keywords

Biomass-fired powerplants, austenitic stainless steel, creep, fatigue, thermomechanical fatigue and ageing.

Biomasseldade krafverk, austenitiska rostfria stål, kryp, utmattning, termomekaniskutmattning och åldring.



## Sammanfattning

Projektet ingår som en del i industriinitiativet och forumet KME. Med ökande krav på förbättrad kryp- och utmattningsstyrka, från ökad ångdata samt antal start-och-stopp-cykler, är de nuvarande använda ferritiska stålen i tjockväggiga komponenter i högeffektiva biomasseldade kraftverk inte tillräckliga.

Från tidigare studier har avancerade värmetåliga austenitiska rostfria stål (A-ASS) visat sig vara en lovande kandidat, med hög tillförlitlighet och mer kostnadseffektiv jämfört med annat kandidatmaterial, såsom nickelbaserade legeringar. Det krävs emellertid fler undersökningar för att verifiera att tjockväggiga AASS har tillräcklig säkerhet och tillförlitlighet jämfört med de material som används idag, såsom de ferritiska stålen P91 och P92. Mekaniskt beteende som kryp, utmattning och termomekanisk utmattning (TMF) har undersökts på åldrade material för att simulera långvarig användning.

Kandidatmaterialen uppvisade att åldringen har en skadlig effekt på TMFprestandan. Reduceringen av TMF-prestanda tillskrevs en accelererad mikrostrukturell utveckling som minskade effektiviteten att hindra dislokationsrörelse. Sanicro 25 uppvisade en bättre TMF-prestanda och högre hållfasthet jämfört med Esshete 1250, inklusive jungfruliga och åldrade material. Detta tillskrevs effektiva härdningsmekanismerna vid höga temperaturer hos Sanicro 25. De två legeringarna uppvisade olika sprickpropagerings- och utmattnings- och krypbeteenden, främst på grund av de olika mikrostrukturella utvecklingsbeteendena. I Sanicro 25 fungerade koherenta Cu-rika utskiljningar och icke-koherenta Nb-karbider som dislokationshinder och bidrar därför till Sanicro 25s effektiva härdningsbeteende och högtemperaturegenskaper. Esshete 1250 upplevde enbart sprickpropagering längs korngränserna. En ny utmattnings- och krypsprickpropageringsprocess hos Sanicro 25 föreslogs, vilket involverade dynamisk rekristallisation (DRX) av den plastiska zonen vid sprickspetsen. Kandidatmaterialens utskiljningsbeteende samt dess inverkan på deformations-, skade- och brottmekanismerna har utvärderats i projektet. På grund av de otillfredsställande svetsresultaten kunde emellertid segheten hos svetsade och åldrade material inte utvärderas.

Utöver ovan har projektet visat att Sanicro 25 skulle kunna användas för att minska vikten av kraftverkskomponenterna med bibehållen säkerhet, jämfört med nuvarande material.

Projektet resulterade i ny kunskap och förståelse för de två austenitiska rostfria stålens mekaniska och mikrostrukturella utveckling under TMF, utmattning och krypbelastning samt strukturell stabilitet när det gäller utskiljningar. Denna nya kunskap kan användas som bas för materialval med avseende på framtida användning av dessa material i tjockväggiga komponenter i biomassaeldade kraftverk. Dessutom kan den nya kunskapen och förståelsen användas för materialutveckling och till viss del lättare kraftverksdesign.



## **List of content**

1	Background								
	1.1	Goal	10						
2	Project plan								
	2.1	Materials	11						
	2.2	Thermomechanical fatigue testing							
	2.3	Fatigue behaviour and creep resistance							
	2.4	Influence of welding and ageing on toughness							
	2.5	Design feasibility study							
	2.6	Co-operation, communication, dissemination and reporting							
3	Results								
	3.1	Thermomechanical fatigue testing							
		3.1.1 Mechanical response during TMF of virgin and age	ed materials 14						
		3.1.2 Microstructural evolution after TMF testing of virg materials	gin and aged 17						
	3.2	Fatigue behaviour and creep resistance	22						
		3.2.1 Mechanical response during fatigue and creep tes and aged materials	ting of virgin						
		3.2.2 Microstructural evolution after fatigue and creep	testing 25						
	3.3	Influence of welding and ageing on toughness							
	3.4	Design feasibility study							
	3.5	Co-operation, communication, dissemination and reporting	ng 33						
4	Discu	ussion	34						
5	Publi	Publication list							
6	Refe	erences	37						



## 1 Background

Biomass is the largest global contributor to renewable energy and has a great potential to expand in the production of heat and electricity [1]. It is a sustainable fuel because it gives no net contribution of CO<sub>2</sub> to the atmosphere and it can be considered endless [1, 2]. However, the global increase in energy consumption and the increase in emissions of greenhouse gases (e.g. CO<sub>2</sub>) causing global warming, make needs for both an increase in energy production and a reduction of greenhouse gas emission [3, 4]. One way to accomplish both needs is to increase the efficiency of biomass-fired power plants, which could be reached by increasing temperature and pressure in the boiler sections and consequently in other components of the system, such as headers and piping [5]. Thus, the requirement of more energy production is met and since biomass has no net contribution of CO<sub>2</sub> to the atmosphere less emissions of greenhouse gases is the result.

The heavy section materials used as headers and piping in the future high-efficient biomass-fired power plants are required to display improved properties such as higher creep and fatigue strength and high-temperature steam oxidation resistance. The performance of heavy section A-ASS at these elevated temperatures is not yet fully understood [6, 7]. From previous project (SEA project number 39297-1) [8] A-ASS materials, such as Sandvik Sanicro™ 25 (Sanicro 25), have showed to be promising candidates, with high reliability. In addition, they are more cost-effective compared to nickel-based alloys that are other candidates for components in high-efficient biomass-fired power plants. However, more investigations are needed to verify that heavy section A-ASS materials have the sufficient safety and reliability.

Since the lifetime of power plant is expected to be 30 years or more [9], materials with better long term high-temperature performances, as safety and structural integrity [10], are desirable. The influence of long-term high-temperature exposure as well as the combination of welding and long-term high-temperature exposure on toughness for heavy section A-ASS are not known. Welding is of interest since it is an important joining process both for headers and piping as well as for repair of damage from, for example steam oxidation. In addition, more knowledge is needed to verify that heavy section A-ASS are a long-term solution for headers and piping in biomass-fired power plants with increased steam data.

Biomass-fired power plants are supposed to withstand many start and stop cycles to maintain efficiency in the global energy and electricity network. This advocates for investigations of how cyclic operation conditions influence the high-temperature performance of heavy section A-ASS. One way to investigate the cyclic high-temperature properties of the candidate materials is to study the thermo-mechanical fatigue (TMF) behaviour [11]. For a heavy section component, temperature gradients are an issue, since the temperature gradient will cause problems related to the thermal expansion. TMF testing in out-of phase (OP) condition will have a temperature profile that simulate the real conditions for a hot-spot surrounded by colder material or the hot-side of a thicker wall with a temperature gradient. OP testing in TMF means that the mechanical strain is in



compression when the temperature is high and vice versa. However, this is a topic where very little research has been conducted [12].

With the new operation conditions fatigue crack propagation behaviour becomes more important for heavy section materials used for headers and piping. However, the fatigue crack propagation behaviour is not well known for these new heavy section A-ASS materials. Thus, there is a need of fatigue crack propagation testing to verify the safety of the material.

#### 1.1 **GOAL**

Increasing the efficiency of a biomass power plant is obtained mainly by increasing temperature and pressure. The material used will suffer from a tougher environment resulting in safety and reliability problems. The main purposes of this project are to evaluate the mechanical behaviours for structure safety and integrity analysis, namely:

- 1) To evaluate thermo-mechanical fatigue properties of new header and piping materials for safety and life evaluation since the biomass-fired power plants can start/shutdown quite often during service for energy saving and flexibility purposes in the future.
- 2) To evaluate the fatigue crack propagation behaviour of new header and piping materials used in safety and reliability considerations since the header and pipe material can undertake low cycle fatigue during the service.
- 3) To evaluate the creep resistance of new header and piping materials used in safety and reliability considerations since the header and pipe material can undertake creep during the service.
- 4) To evaluate the structure stability and the toughness of welded and aged material after long term service at high temperatures for safety analysis.
- 5) To evaluate the new candidate material compared to currently used materials using FE-models of the applications.

The main industrial goal is to verify the safety and reliability of heavy section Sandvik Sanicro™ 25 (Sanicro 25) to be used as new potential better material for headers and piping in biomass-fired power plants. The main academic goals are to produce one technical doctor as well as publication of articles on the new findings from the project, such as mechanical and microstructural characterisation of the new heavy section material.



## 2 Project plan

To with confidence reveal if A-ASS is a possible candidate for long-term service in high-efficiency biomass-fired power plants a more in-depth evaluation of creep resistance, TMF properties, fatigue crack propagation mechanisms and the influence of structure stability on toughness is needed. The project plan consists of the following five parts including testing and material characterisation to fulfil the project goals.

#### 2.1 MATERIALS

The materials of interest are Sanicro 25 and Esshete 1250 in different conditions. Currently used ferritic stainless steels, such as P91 and P92, will be used as reference materials. See table 1 for the chemical compositions of the tested materials. The Sanicro 25 and Esshete 1250 materials were supplied by Sandvik and the P91 and P92 materials were supplied by Sumitomo.

Table 1: Chemical composition of the tested austenitic stainless steels.

Material	C	Cr	Ni	W	Co	Cu	Mn	Nb	N	Si	$\mathbf{v}$	Mo	Fe
Sanicro 25	0.1	22.5	25.0	3.6	1.5	3.0	0.5	0.5	0.23	0.2	-	-	Bal.
Esshete 1250	0.1	15	9.5	-	-	-	6.3	1.0	-	0.5	0.3	1.0	Bal.

#### 2.2 THERMOMECHANICAL FATIGUE TESTING

Thermomechanical fatigue (TMF) testing has been performed on Sanicro 25 and Esshete 1250 in different conditions to fulfil the first project goal. This simulates flexible operation conditions of the future high-efficient biomass-fired power plants with many start-and-stop cycles. Long-term ageing was performed on the materials. By performing long-term ageing at up to 700 °C for up to 10 000 hours, the effect of service degradation will be considered. The resistance to TMF failure was analysed and compared for the different material conditions. The maximum temperature in the tests will be up to 700 °C and performed in OP condition. Different microscopy techniques were used to analyse the microstructural evolution such as deformation and damage mechanisms.

#### 2.3 FATIGUE BEHAVIOUR AND CREEP RESISTANCE

Fatigue crack propagation behaviour and creep resistance were studied for Sanicro 25 and Esshete 1250 in different conditions and will fulfil the second and the third project goal. Long-term ageing was performed on the materials. By performing long-term ageing up to 700 °C for up to 10 000 hours the effect of service degradation will be considered. Fatigue and creep testing was performed to study the cracking behaviour due to low cycle fatigue and creep resistance. Sanicro 25 and Esshete 1250 in different material conditions were investigated and compared. Different microscopy techniques were used to analyse the microstructural evolution such as crack propagation mechanisms.



#### 2.4 INFLUENCE OF WELDING AND AGEING ON TOUGHNESS

Welded Sanicro 25 and Esshete 1250 material both virgin and aged were planned to be investigated. By performing long-term ageing at temperatures from 600 °C and up to 700 °C for up to 10 000 hours the effect of service degradation were considered. Welding and combined with ageing could have a significant effect on degradation of the material's structural integrity. This part will fulfil the fourth project goal. Impact and fracture toughness test were planned to be performed after up to 10 000 hours ageing process, using Charpy V and CTOD methods respectively. Different microscopy techniques were planned to be used to analyse the microstructural evolution such as deformation and fracture mechanisms.

#### 2.5 DESIGN FEASIBILITY STUDY

Design feasibility study for relevant systems of the applications for comparison of the new candidate and the currently used materials as well as feedback related to mechanical design. This part will fulfil the fifth project goal. Stress analysis results from Sanicro 25 and Esshete 1250 were compared to P92. This will reveal if the new candidate material is potentially better for selected application system and if design improvements are possible.

# 2.6 CO-OPERATION, COMMUNICATION, DISSEMINATION AND REPORTING

A vital part of the project was the communication of industrial needs to the academic researchers and the dissemination of results from the researchers back to industry.



#### 3 Results

In this section, the results from the project are presented according to the different parts described in the project plan section aligned with the fulfilment of the goals.

#### 3.1 THERMOMECHANICAL FATIGUE TESTING

The thermomechanical fatigue (TMF) in strain control has been conducted to Sanicro 25, Esshete 1250 and P91. Selected results to fulfil the goals of the project from the TMF testing are presented below, both as graphs and the related microstructural evaluation. However, in the PhD thesis by Hugo Wärner [13], the results are presented in detail and all parameters regarding test set up are given. This project focus on OP-TMF, and both mechanical behaviour and microstructural evolution such as deformation, damage and failure mechanisms related to OP-TMF will be presented.

In Figure 1 the different TMF test cycles are explained, as mentioned, in this project OP-TMF has been focused on.

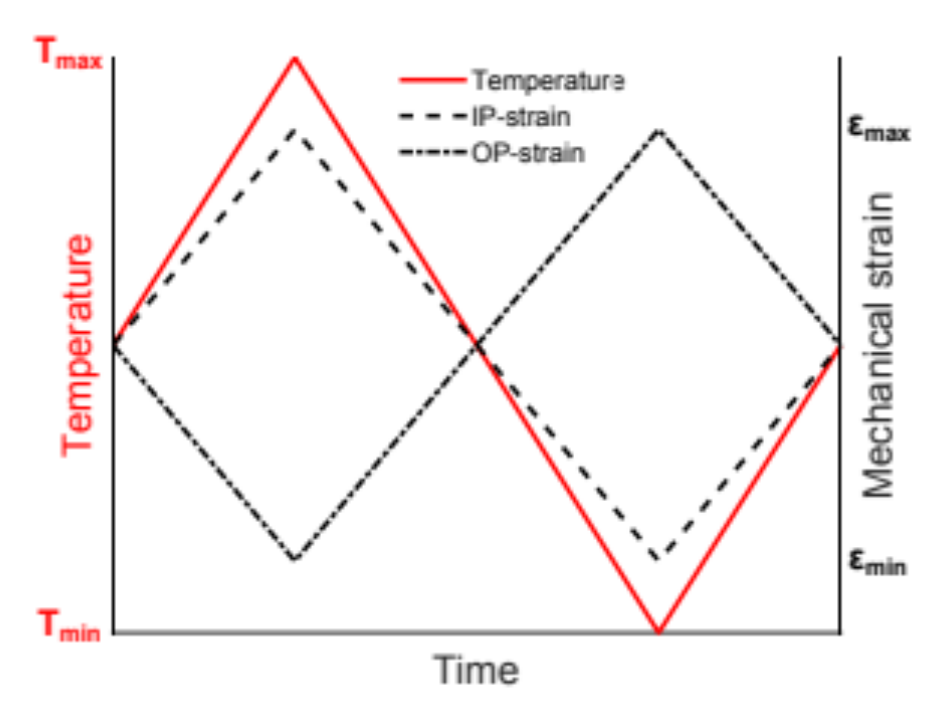


Figure 1: Schematics of the different TMF test cycles.

In Figure 2 the sample geometry that was used during the OP-TMF tests is presented and one example of a test specimen after testing.



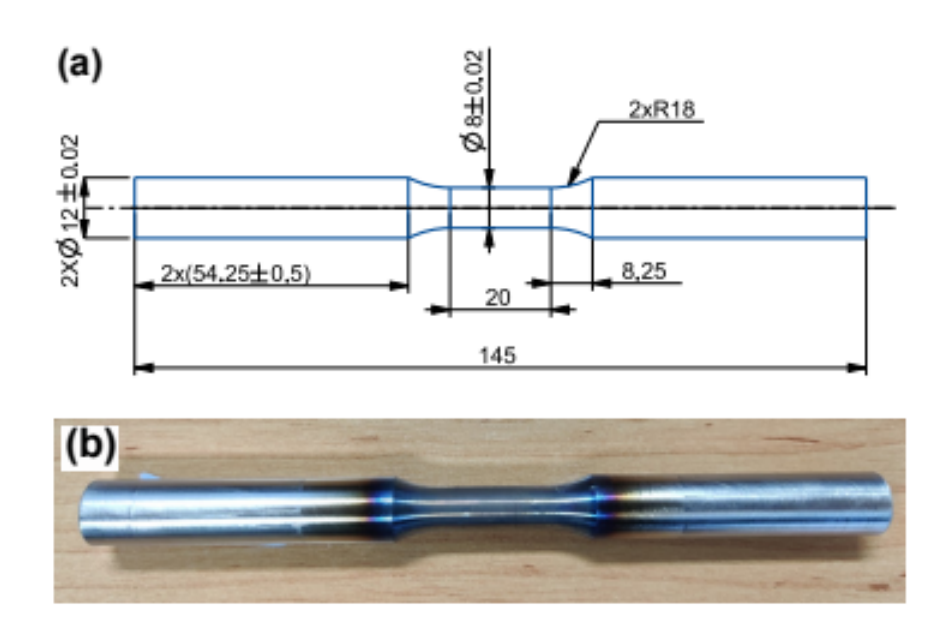


Figure 2: The test specimen, (a) schematics (units in millimeters), (b) after testing of an OP-TMF Ehsshete 1250 specimen.

#### 3.1.1 Mechanical response during TMF of virgin and aged materials

In Figure 3, the mechanical response of virgin and aged Sanicro 25 and Esshete 1250 are presented in the form of stress amplitude vs cycles. It is shown that the Sanicro 25 experience cyclic hardening to a greater extent compared to Esshete 1250. Comparing the OP-TMF response of the two austenitic stainless steels reveals that Sanicro 25 has the better strength and would last longer at higher stresses in an stress controlled loading condition in a power plant component. Ageing has a degrading effect on both alloys, however, Sanicro 25 show more remaining strength after long-term ageing compared to Esshete 1250.

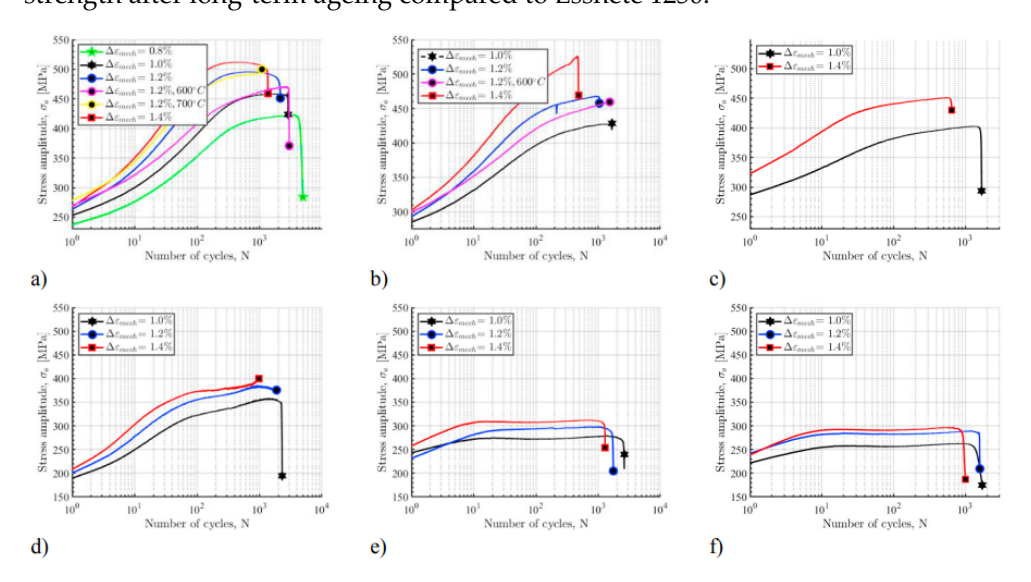


Figure 3: OP-TMF stress amplitude vs cycles curves for Sanicro 25 a) virgin, b) aged (3000 h at 650  $^{\circ}$ C) and c) aged (10 000 h at 650  $^{\circ}$ C) and Esshete 1250 d) virgin, d) aged (3000 h at 650  $^{\circ}$ C) and f) aged (10 000 h at 650  $^{\circ}$ C).



Figure 4 show the mechanical response of virgin P91 in the form of stress amplitude vs cycles. P91 experience a cyclic softening and the stress levels and TMF-life are comparable to the cyclic hardened Sanicro 25. However, Esshete 1250 show a significant lower strength compared to P91.

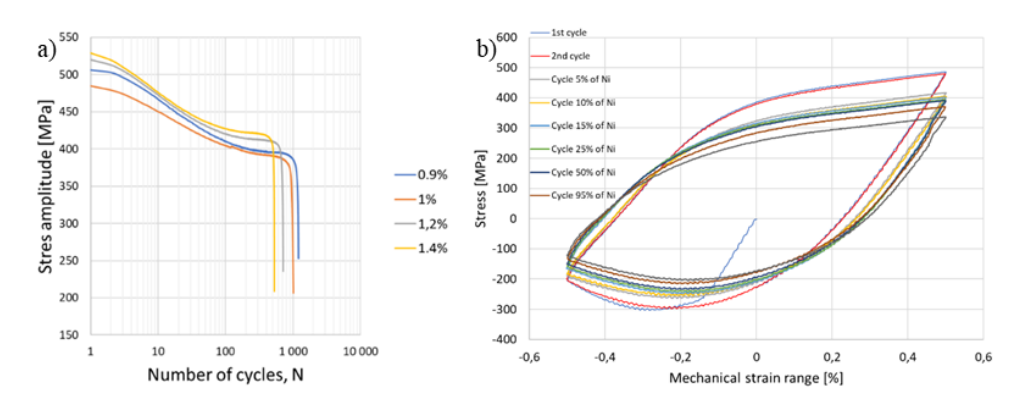


Figure 4: OP-TMF results of virgin P91 a) stress amplitude vs cycles curves and b) hysteresis curves, ΔT = 100–650 °C, Δεmech = 1 %.

Some of the hysteresis curves are shown in Figures 5 and 6 for Sanicro 25 and Figure 7 for Esshete 1250 and Figure 4 b) for P91. For Sanicro 25 the aged specimens experienced increased plastic strain range ( $\Delta\epsilon_P$ ), comparing Figure 5a and Figure 5b at the same percentage of life.

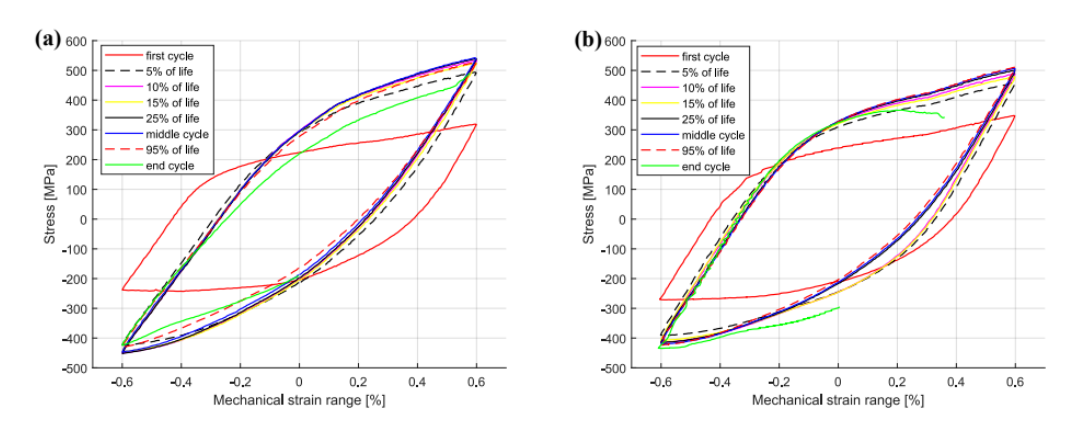


Figure 5: OP-TMF hysteresis curves of Sanicro 25,  $\Delta T = 100-650 \,^{\circ}$ C,  $\Delta \epsilon$ mech = 1.2%, (a) virgin and (b) aged (3 000 h at 650  $^{\circ}$ C).

The reference  $T_{max}$  tests (Figure 6) show similar difference of the plastic strain range as for the 650 °C tests, with increased  $\Delta\epsilon_P$  for the aged specimen (Figure 6b) compared to the virgin specimen (Figure 6a).



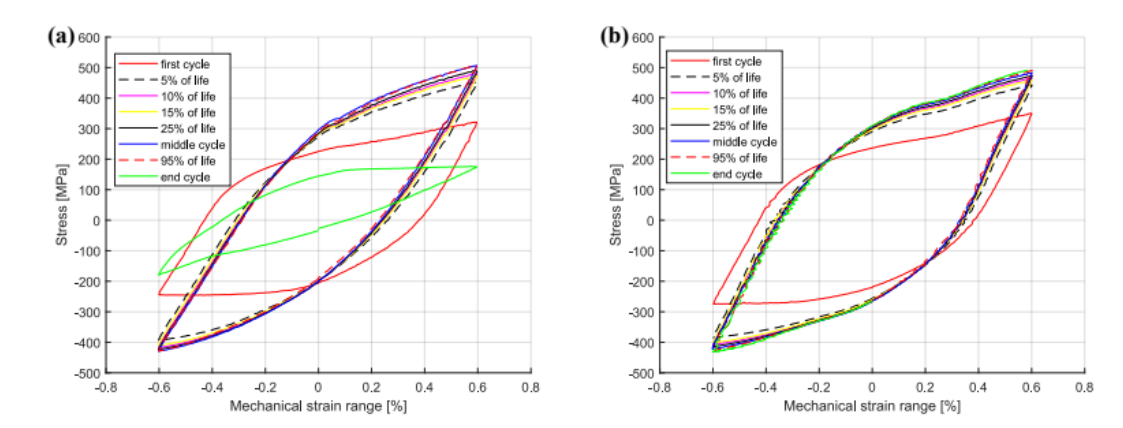


Figure 6: OP-TMF hysteresis curves of Sanicro 25,  $\Delta \epsilon$ mech = 1.2%, (a) virgin,  $\Delta T$  = 100–600 °C and (b) aged (3 000h at 600 °C),  $\Delta T$  = 100–600 °C.

As a consequence of this, the aged specimens also showed increased plastic strain range (Figure 8b), which did not decrease after the initial stage as for the virgin specimens (Figure 8a).

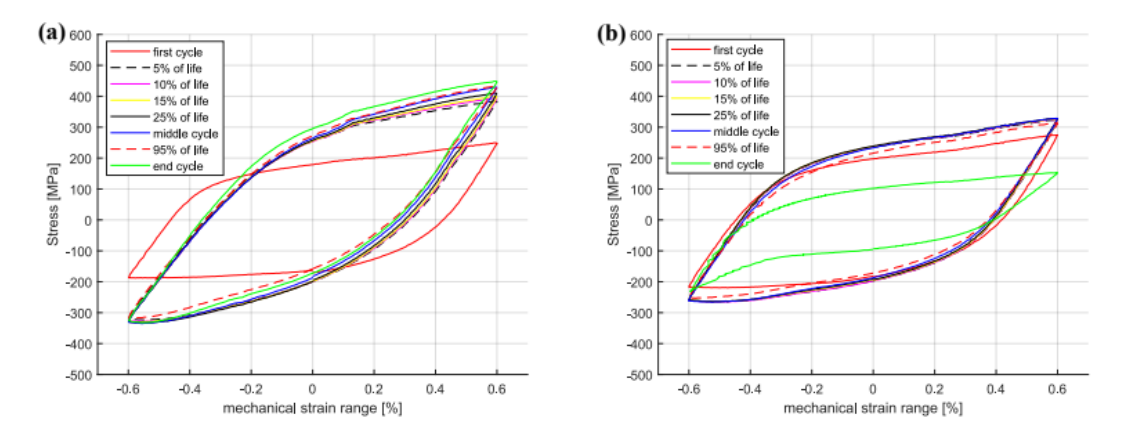


Figure 7: OP-TMF hysteresis curves of Esshete 1250,  $\Delta T = 100-650$  °C,  $\Delta \epsilon$ mech = 1.2%, (a) virgin and (b) aged (3 000h at 650 °C).

In Figure 8 some of the OP-TMF mechanical properties, mechanical strain range vs. number of cycles to fracture and plastic strain amplitude vs. number of cycles, for Sanicro 25 and Esshete 1250 are summarised. With greater applied  $\Delta \epsilon_{mech}$ , the ageing did not clearly negatively affect the OP-TMF life of Esshete 1250 as it did for Sanicro 25 (Figure 8a). Although, the loss of structural integrity induced higher plastic strain range at lower stress levels (Figure 8b). For Sanicro 25 in terms of fatigue life, altering the test temperature for the  $\Delta \epsilon_{mech}$  = 1.2% specimens approximately corresponded to changing the  $\Delta \epsilon_{mech}$  one step (1.0% for 600 °C and 1.4% for 700 °C).



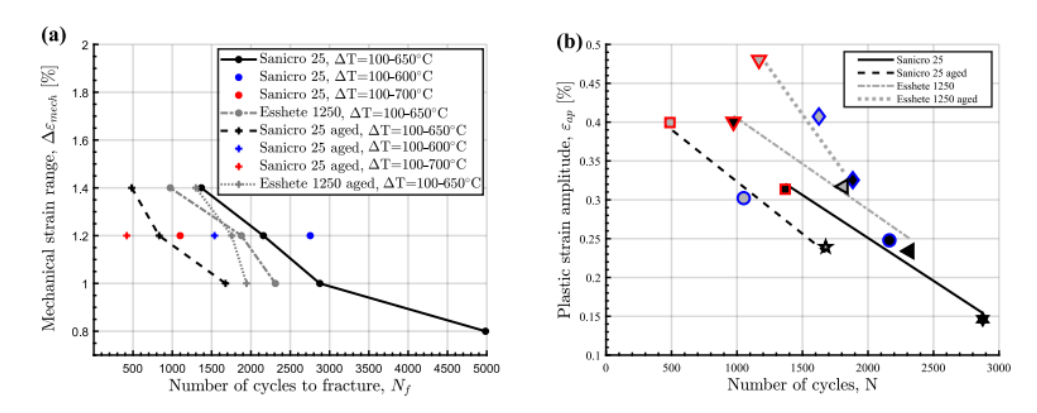


Figure 8: Summation plots of the two investigated austenitic stainless steels, (a) OP-TMF life of the tested specimens, (b) the plastic strain amplitude at OP-TMF midlife in relation to the amount of cycles to fracture,  $\Delta T = 100-650 \, ^{\circ}\text{C}$  (aged = 3 000h at  $T_{\text{max}}$  in the TMF temperature range, meaning 600, 650 and 700  $^{\circ}\text{C}$  respectively).

Another indication of higher plastic strain range at lower stress levels induced by the loss of structural integrity is the Vickers hardness results in Figure 9, where the tested aged specimens show lower hardness than the equivalent tested virgin specimens. All the undeformed specimens have similar hardness level.

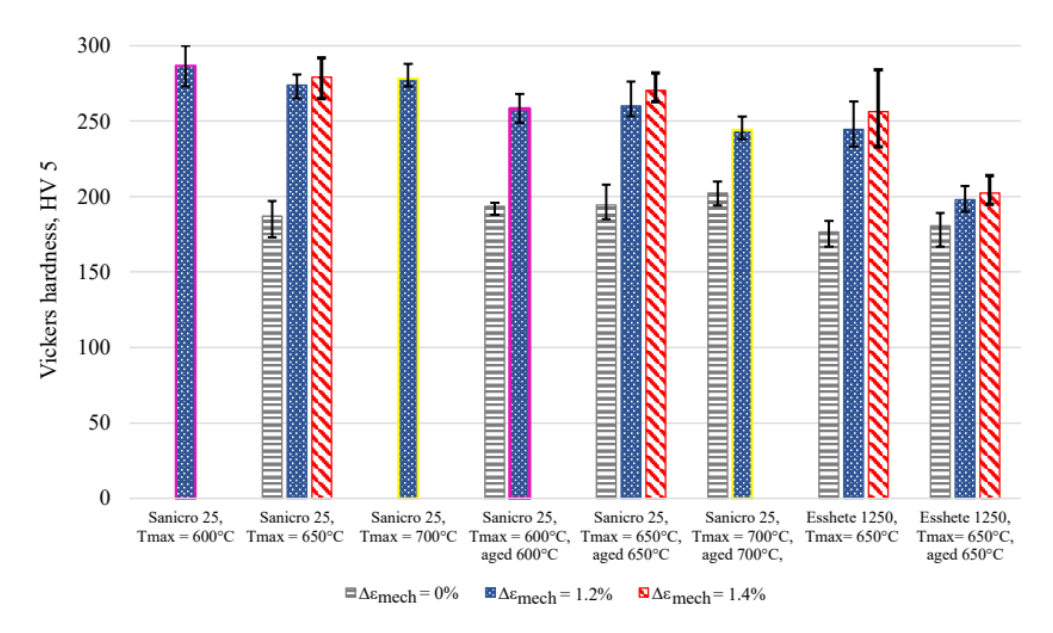


Figure 9: Vickers hardness of the investigated OP-TMF specimens (testing performed at room temperature after TMF cycling).

#### 3.1.2 Microstructural evolution after TMF testing of virgin and aged materials

In Figures 10 and 11 show the microstructure of virgin and aged Sanicro 25 after OP-TMF testing ( $\Delta \epsilon_{mech} = 1.2\%$ ). The virgin specimens did not proceed to complete fracture (complete specimen break) and the main crack seemed to have been propagating transgranularly according to Figure 10b. Many of the bulk material grains show signs of plastic straining, where areas of severe plastic deformation



can be seen at the vicinity of the cracks (Figure 10a and b) and other grains show what appears to be slip formations (Figure 10a). Plastic straining in the form of slip formations is frequently observed during high temperature loadings for these kind of materials [14, 15]. Figure 10c shows a magnified crack tip area of the main crack, which contains high plasticity and precipitates enriched by nitrogen, chromium, and niobium that either cracked during straining or have been detached during the polishing/grinding of the sample. By comparison, the aged Sanicro 25 condition show similar "cracked" precipitates, but in larger sizes and quantities and sometimes precipitates are grouped together occupying relatively big areas (Figures 11a and 12), with the bigger precipitates in the middle and with smaller precipitates at its boundaries.

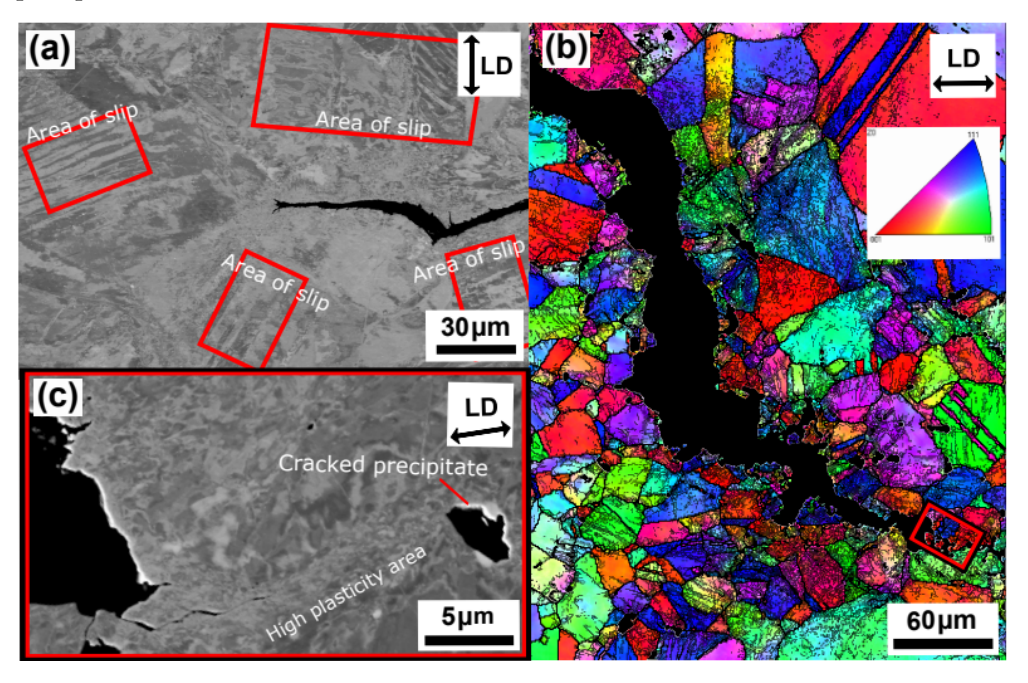


Figure 10: Micrograph of virgin Sanicro 25,  $\Delta T = 100-650$  °C,  $\Delta \varepsilon_{mech} = 1.2\%$ , (a) BSE analysis of secondary initiation overview, (b) EBSD analysis of the main crack, (c) enlarged BSE image of the crack tip in (b).



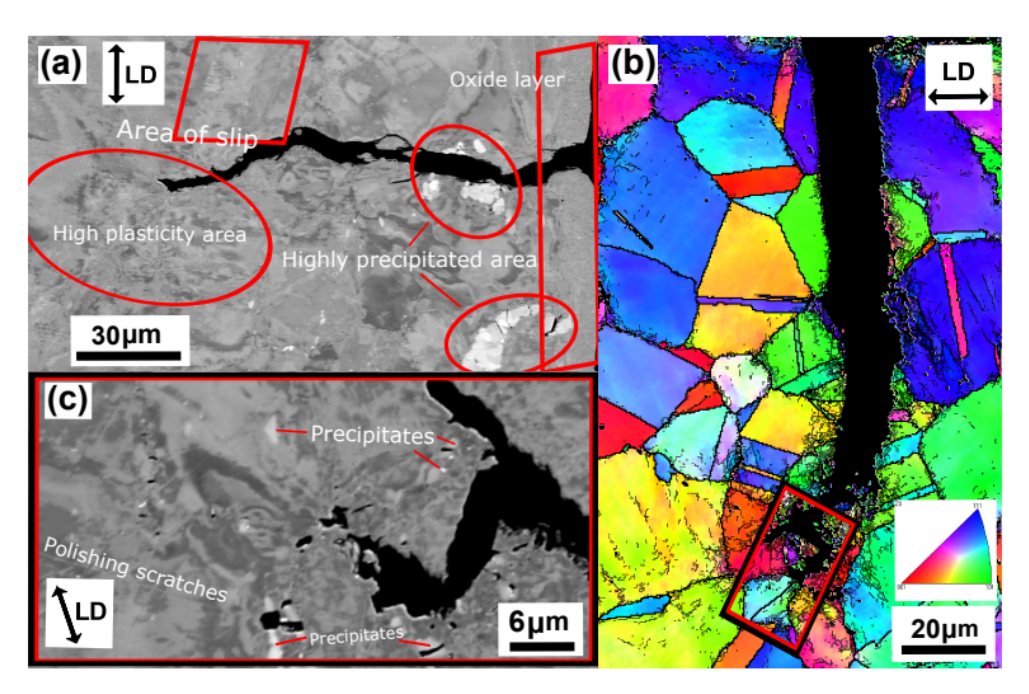


Figure 11: Micrograph of aged (T = 650 °C) Sanicro 25,  $\Delta T$  = 100–650 °C,  $\Delta \epsilon_{mech}$  = 1.2%, (a) BSE image of a secondary initiation overview, (b) EBSD analysis of a secondary crack initiation, (c) enlarged BSE image of the crack tip in (b).

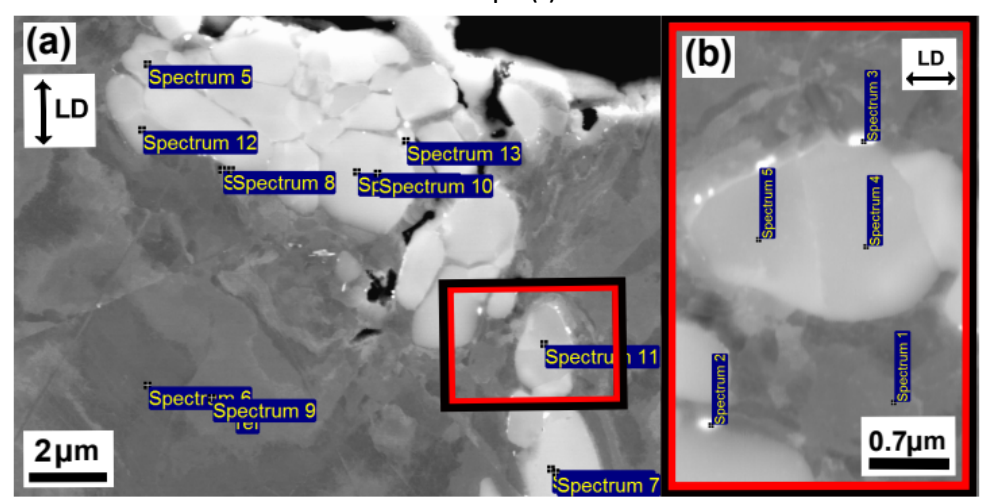


Figure 12: Micrograph of aged Sanicro 25,  $\Delta T = 100-650\,^{\circ}C$ ,  $\Delta \epsilon_{mech} = 1.2\%$ , (a) BSE image which show the EDS point spectrum positions of the highly precipitated region in the middle of the crack in Figure 11a, (b) enlarged BSE image which show the EDS point spectrum positions (zoomed image in (a)).

With EDS it is hard to identify these grouped precipitates given the resolution of the technique, but these areas show enrichment of niobium, chromium, carbon, nitrogen, copper, and tungsten, as evident by the spectrum quantitative results in Table 2.



Table 2: The quantitative EDS spectrum results (in wt.%) of the aged Sanicro 25 microstructure in Figure 12.

		-		-			_
Spectrums	С	Cr	N	Ni	Cu	Nb	W
Figure 12a							
Spectrum 5	6.7	25.7	4.2	5.2	0.7	44.5	3.6
Spectrum 6/9 (ref)	3.3	22.2	0.5	24.0	2.8	0.4	3.6
Spectrum 7	5.9	27.0	3.7	0.6	0.2	57.5	4.3
Spectrum 8	6.7	24.0	0.9	14.1	7.5	16.9	4.7
Spectrum 10	6.9	26.9	4.4	1.1	0.2	56.3	3.8
Spectrum 11	6.0	27.9	5.6	2.2	0.3	52.5	3.5
Spectrum 12	5.3	23.3	1.5	12.3	1.4	29.0	4.0
Spectrum 13	7.2	25.3	2.4	4.3	0.6	47.8	4.6
Figure 12b (enlarged image)							
Spectrum 1 (ref)	4.7	20.6	0.4	23.3	3.5	0.7	3.2
Spectrum 2	5.9	20.1	2.5	14.3	1.3	22.9	7.9
Spectrum 3	7.7	24.1	2.1	10.0	1.3	31.6	5.0
Spectrum 4	9.8	25.7	5.2	2.5	0.3	50.0	4.0
Spectrum 5	10	27.9	4.9	2.9	0.4	46.9	2.9

The virgin Esshete 1250  $\Delta\epsilon_{mech}$  = 1.2% specimen, also suffered complete fracture (complete specimen break) and, similar to the Sanicro 25 specimens, the probable propagation type is also transgranular. This is found when investigating secondary initiations, such as in Figure 13b. Figure 13a shows a crack branch connected to the fracture surface of the main crack. Both sides of the crack branch give evidence of plastic straining, most likely in the form of slip areas, which supports crack growth. The close-up image of the crack branch midsection, shown in Figure 13c, indicates that the crack propagation is also influenced by cracking of precipitates. The corresponding aged specimens exhibit areas of the same precipitates that were identified as niobium carbides (NbCs) given the quantitative data in Table 3. In addition, similar evidence of severe plastic straining close to the crack tips can be seen in Figures 14a–c and 15a and b. However, in contrast to the virgin specimens, the aged specimens did not suffer full fracture (complete specimen breakage). Instead, there were one main crack with crack branching and comparably fewer secondary initiations. These are presented in Figure 14b.



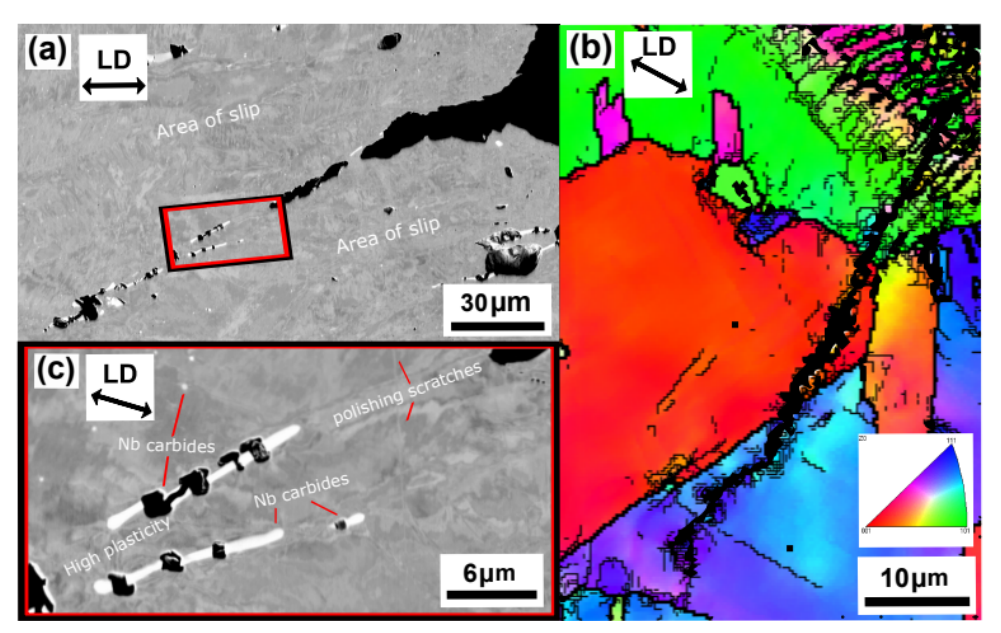


Figure 13: Micrograph of virgin Esshete 1250, ΔT = 100–650 °C, Δεmech = 1.2%, (a) BSE image of crack branching from the main crack, (b) EBSD analysis of a secondary crack initiation, (c) enlarged BSE image of the crack midsection in (a).

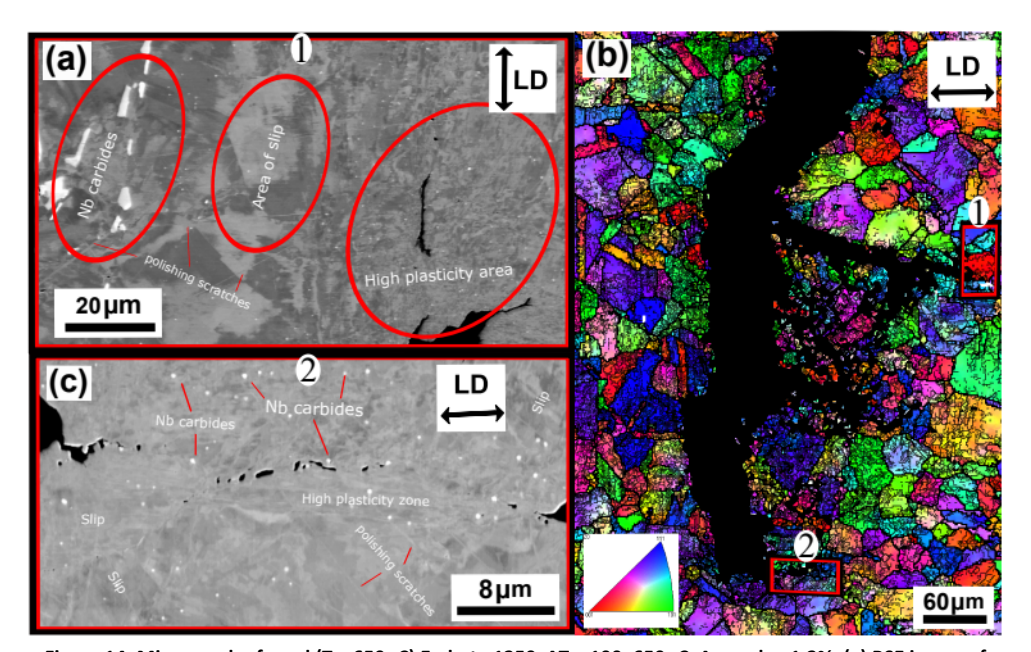


Figure 14: Micrograph of aged (T = 650 °C) Esshete 1250, ΔT = 100–650 °C, Δεmech = 1.2%, (a) BSE image of crack branching from the main crack (zoomed image 1 in (b)), (b) EBSD analysis of the main crack initiation, (c) enlarged BSE image of the crack tip (zoomed image 2 in (b)).

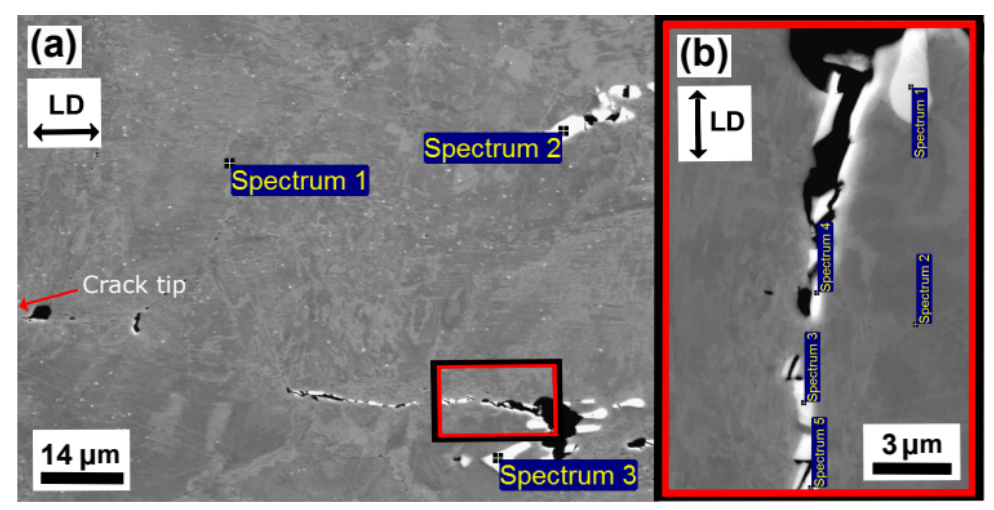


Figure 15: Micrograph of aged Esshete 1250, ΔT = 100–650°C, Δε<sub>mech</sub> = 1.2%, (a) BSE image which show the EDS point spectrum positions of the region in front of the crack tip (the area in front of Figure 14c,"(2)"), (b) enlarged BSE image which show the EDS point spectrum positions (zoomed image in (a)).

Table 3: The quantitative EDS spectrum results (in wt.%) of the aged Esshete 1250 microstructure in Figure 15.

Spectrums	C	Cr	Mn	Fe	Ni	Nb	Mo
Figure 15a							
Spectrum 1 (ref)	2.9	15.4	7.2	61.0	9.8	0.9	1.4
Spectrum 2	16.4	4.1	1.6	12.9	1.6	62.7	0.1
Spectrum 3	6.7	11.1	4.6	43.6	6.1	26.3	0.9
Figure 15b (enlarged image)							
Spectrum 1	18.3	1.4	0.5	3.3	0.41	75.1	0.3
Spectrum 2 (ref)	2.8	15.3	6.7	63.5	9.2	0.5	1
Spectrum 3	5.56	17.0	5.5	47.9	6.9	14.7	1.7
Spectrum 4	4.21	13.2	6.1	58.8	8.3	7.5	0.9
Spectrum 4	4.5	13.1	5.9	55.8	8.0	10.8	0.9

#### 3.2 FATIGUE BEHAVIOUR AND CREEP RESISTANCE

Fatigue and creep testing have been conducted on the investigated austenitic stainless steels. The fatigue part was under strain control and the creep part under load control. Results have been selected to show the fulfillment of the goals of the project, including both graphs of mechanical response and the related microstructural evaluation. However, in the PhD thesis by Hugo Wärner [13], the results are presented in detail and all parameters regarding test set up are given.

# 3.2.1 Mechanical response during fatigue and creep testing of virgin and aged materials

The materials studied were Sanicro 25 and Esshete 1250. Sanicro 25 had an average initial grain size of ASTM 3.8 (average diameter of 26.9  $\mu m$ , but larger grains up to 150  $\mu m$  were seen in the microstructure) and Esshete 1250 had an average initial grain size of ASTM 4.3 (average diameter of 21.6  $\mu m$ , but larger grains up to 100  $\mu m$  were seen in the microstructure). The chemical compositions of the investigated materials in wt% can be seen in Table 1. The geometry of used specimens is shown in Figure 16. The isothermal fatigue and creep testing at up to



700 °C was conducted as shown in Figure 17, with strain-controlled fatigue part (black dotted line) and load controlled creep part (black solid line). The number of cycles to failure (N<sub>f</sub>) was defined as the point where the maximum stress range ( $\Delta\sigma$ ) decreases 10%.

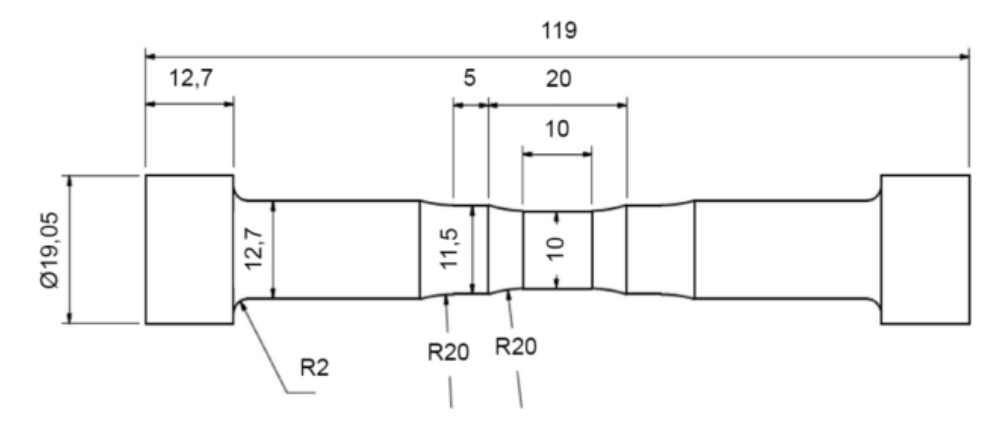


Figure 16: Schematics of the test specimen (units in millimetres).

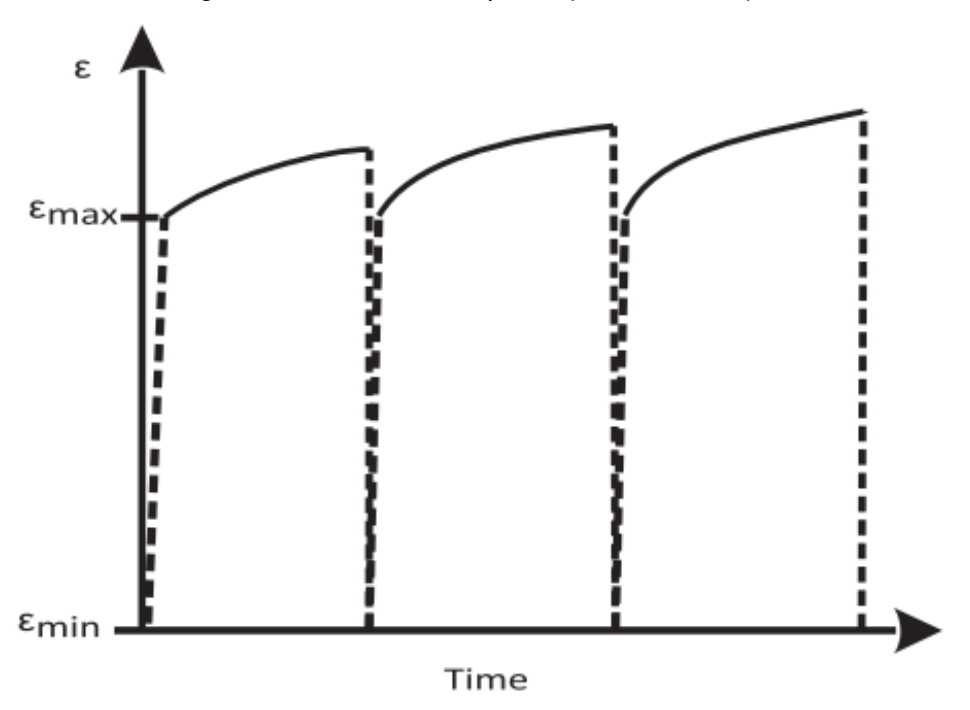


Figure 17: Sketch of the fatigue and creep test cycle. The solid lines represent the load controlled (creep) parts and the dotted lines represents the strain controlled (fatigue) parts.

The fatigue and creep performance focusing on the creep resistance during the dwell time of the two investigated materials are summarised in Figure 18. Clearly there is a difference in creep resistance of the two materials where the creep strain (referring to the accumulated strain during the constant load part (solid line) in Figure 17) at mid life,  $\epsilon_c$  (N<sub>f</sub>/2), are lower for the Sanicro 25 tests, although the maximum stresses at mid life,  $\sigma_{max}$  (N<sub>f</sub>/2), are higher than for equivalent Esshete 1250 tests.



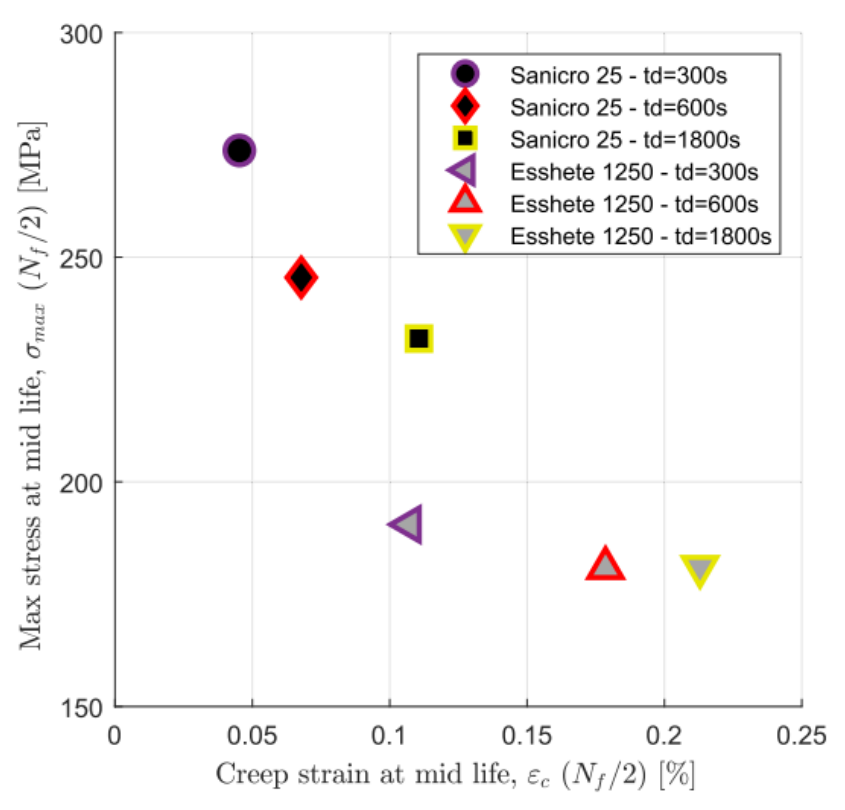


Figure 18: Mechanical response of the investigated conditions,  $\Delta\epsilon/2$  = 0.25%

The hysteresis curves in Figure 19 and Figure 20 show the evolution of the plastic response and the creep straining for both material test extremes, i.e. the tests with the shortest and the longest dwell time, td. Figure 5 a and b both show prominent hardening, from the beginning of the test to 25% of the fatigue and creep life for the two Sanicro 25 test conditions. As indicated in Figure 18, the maximum stress of the  $t_d$  = 1800 s test, is generally lower due to increased creep damage during the longer dwell time.

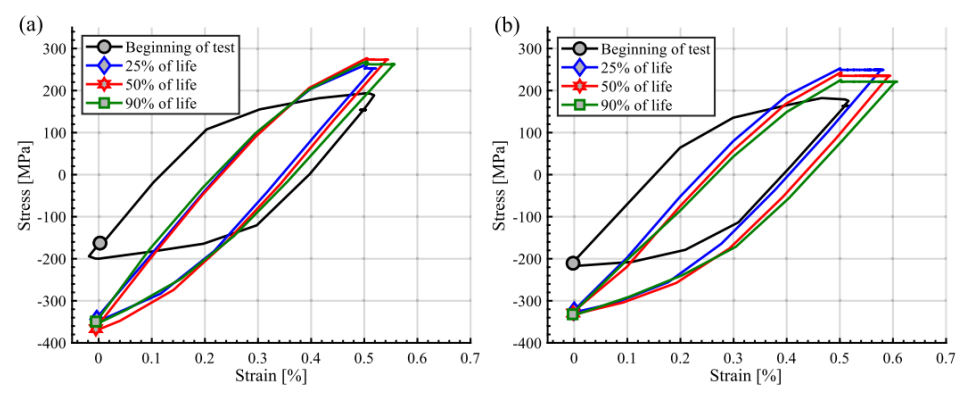


Figure 19: Hysteresis curves of Sanicro 25; (a)  $t_d$  = 300 s, (b)  $t_d$  = 1800 s

During the fatigue and creep life the Esshete 1250 test extremes both show increasing plastic strain range,  $\Delta\epsilon_P$ , as shown by Figure 20 a and b. Compared to the Sanicro 25 tests, the hardening in the first fatigue and creep life quarters is not as prominent. As can be seen in Figure 18, longer  $t_d$  yield increased  $\epsilon_c$  (N<sub>f</sub>/2), for both materials.



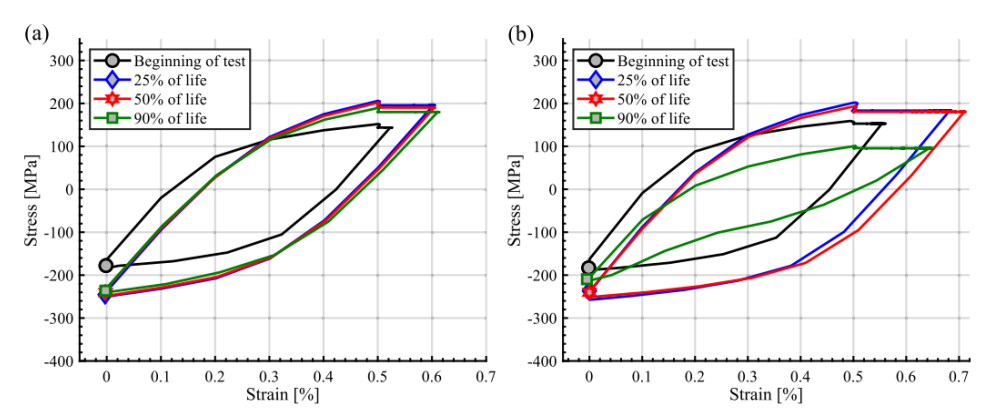


Figure 20: Hysteresis curves of Esshete 1250; (a)  $t_d$  = 300 s, (b)  $t_d$  = 1800 s.

#### 3.2.2 Microstructural evolution after fatigue and creep testing

In Figure 21 the microstructure of a Sanicro 25 test with the longest dwell time can be seen. From the crack overview in Figure 21 a, the crack path is highly branched and interconnected with secondary cracks. In Figure 21 b intergranular cavities can be observed in the region close to the transgranular crack path. Due to the existence of those grain boundary cavities, the transgranular crack path was perturbed and turned intergranular. In addition, the EBSD analysis in Figure 21 c shows that the behaviour of the crack paths is most irregular, alternating between transgranular and intergranular and the sites indicated in the figure shows the creep-initiated grain boundary cavity sites. These sites are also commonly associated with areas of smaller average grain sizes. The microstructures of the Sanicro 25 t<sub>d</sub>=600 s test, Figure 22, also show similar characteristics and with high plasticity in the vicinity of the cracks, even though the branching is not as appreciable. In Figure 22 a the magnified highly plasticised area, show recrystallized grains at the vicinity of the crack path, where fully recrystallized grains are indicated by blue, highly deformed structures are indicated by red and low deformation level structures are indicated by yellow (RX-image). Figure 22 b show transgranular crack interaction with areas of creep initiated damage, but these are less numerous compared to the t<sub>d</sub>=1800 s test. The reduced accumulation of life limiting creep-fatigue interaction damage is therefore attributed to the decreased amount of possibilities for the fatigue driven crack path to link up with the creep-initiated grain boundary cavities. Precipitates and dislocation structures can be seen in Figure 23 and Figure 24. The EDS analysis in Figure 23 a show increased amount of chromium, nitrogen, copper and niobium and the pattern of the analysis indicates that there are most likely Z-phase (CrNbN), Nb-carbides and copper-rich precipitates located around and on the grain boundaries. There are also numerous small black circular spots that do not show any elemental enrichment and are most probably holes of removed precipitates due to etching of the TEM-sample. The dislocation structure and pile up close to a grain boundary are presented in Figure 23b where the increase in dislocation density close to the grain boundary can be seen.



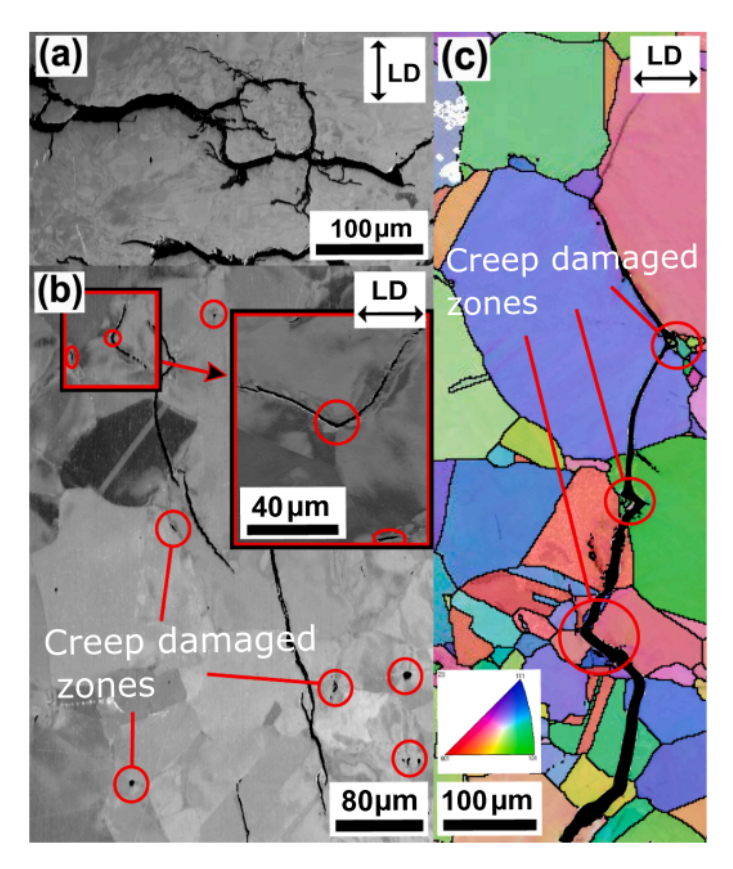


Figure 21: Crack overview of Sanicro 25,  $t_d$  = 1800 s; (a) middle of the crack path, (b) and (c) at the end of the crack path.

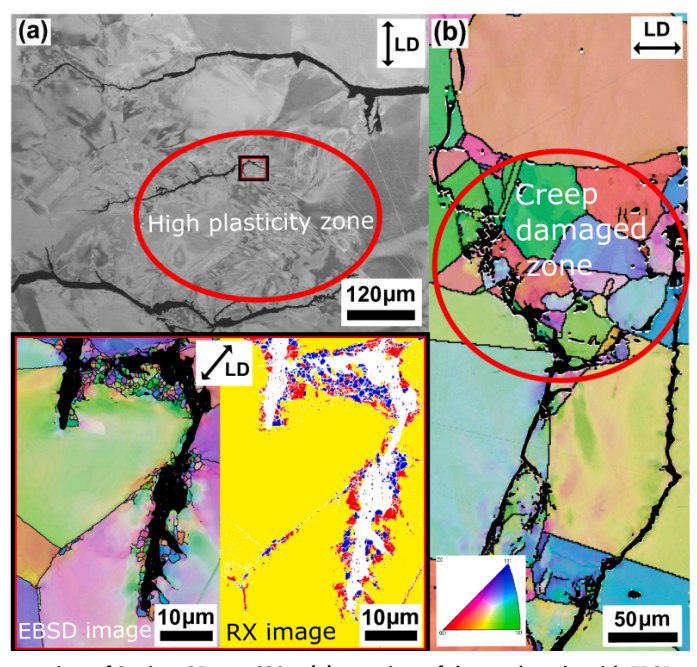


Figure 22: Crack overview of Sanicro 25,  $t_d$  = 600 s; (a) overview of the crack path, with EBSD and recrystallized fraction analysis of a zoomed in area of a highly plasticised zone containing a crack tip, (b) at the end of the crack path.



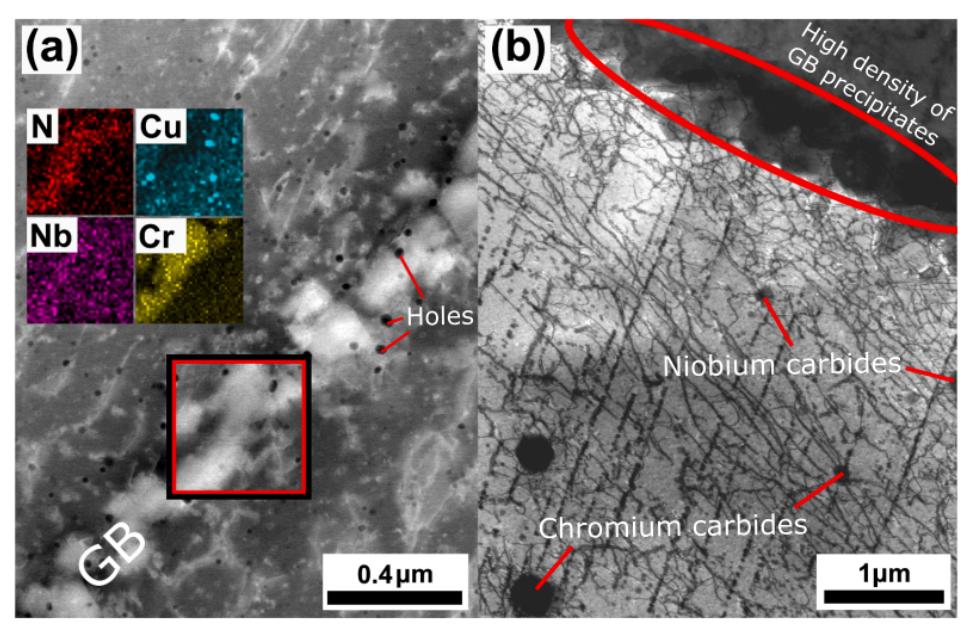


Figure 23: Dislocation structure and grain boundary precipitates of Sanicro 25, t<sub>d</sub> = 600 s; (a) STEM dark field imaging and EDS-analysis of grain boundary precipitates, (b) STEM bright field imaging of dislocation structures and dislocation pile ups in the vicinity of a grain boundary.

In addition, there are Nb- and Cr-carbides in roughly 100 nm-scale in the interior of the grain. In Figure 24, close up images of the deformation structure show very small precipitates that interact with the dislocation arrangements. From EDS-analysis these precipitates are identified as Cr-carbides shown in Figure 24 a, Nb-carbides shown in Figure 24 b and copper-rich precipitates shown in Figure 24 b.

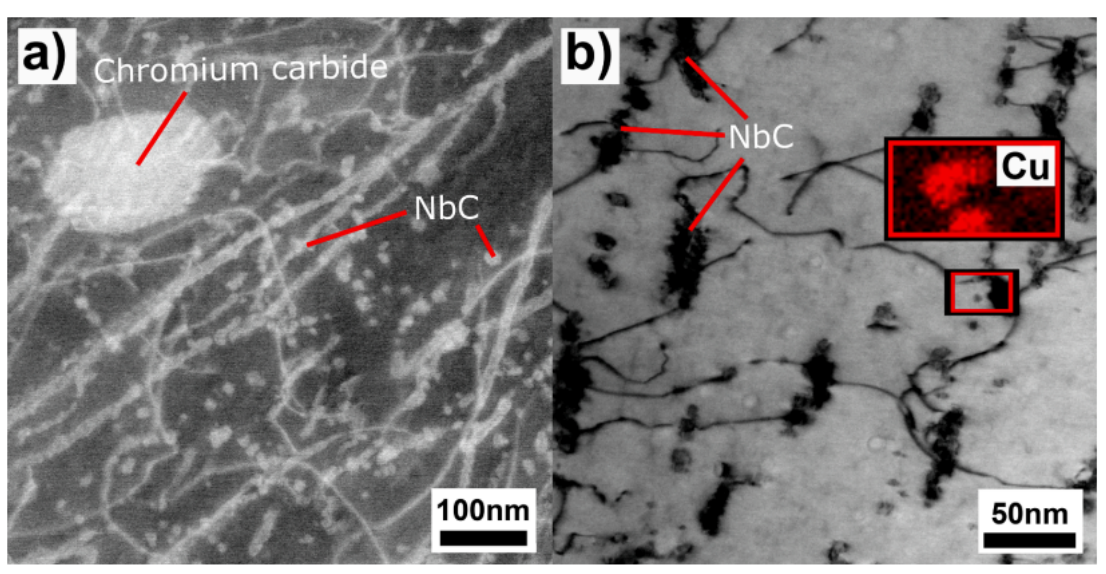


Figure 24: Dislocation and precipitate interaction at nanometre scale of Sanicro 25,  $t_d$  = 600 s; (a) STEM dark field imaging, (b) STEM bright field imaging and EDS-analysis.

The Esshete 1250 tests also showed increased accumulation of  $\epsilon_c$  at N<sub>i</sub>/2 with increasing dwell time (Figure 18) and as mentioned before, all these tests show higher  $\epsilon_c$  at N<sub>i</sub>/2 compared to the equivalent Sanicro 25 tests. By analysing the micrographs of the tests with t<sub>d</sub>=600 s and t<sub>d</sub>=1800 s (Figure 25 and Figure 26 a-c) it is obvious that the crack propagation is associated with damage in the grain boundaries.



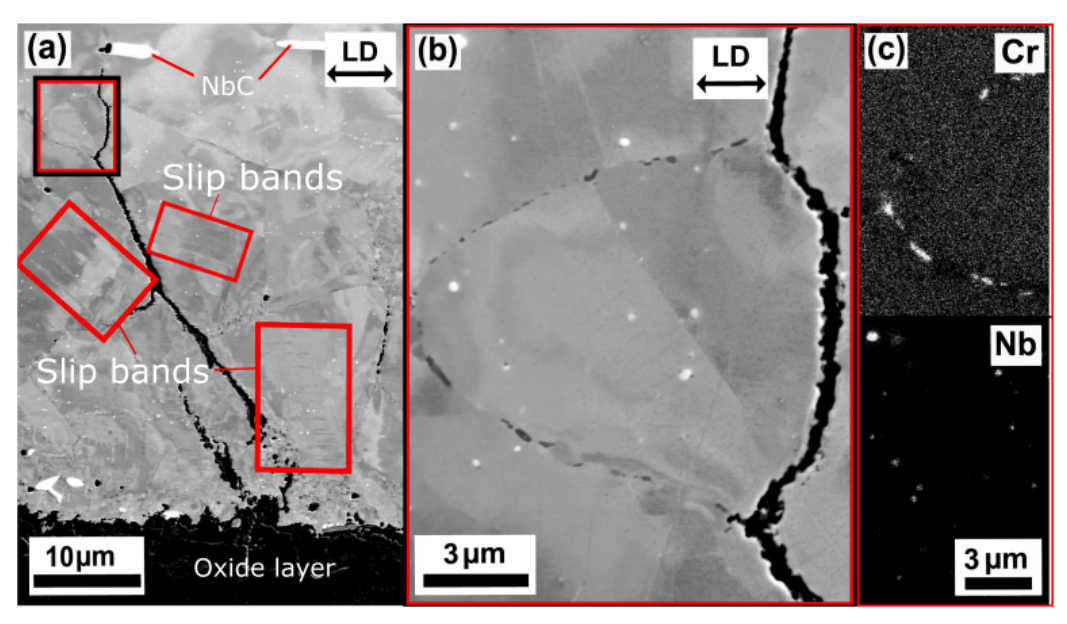


Figure 25: Crack overview at the specimen surface of Esshete 1250,  $t_d$  = 1800 s; (a) crack path overview, (b) zoomed in area in (a), (c) WDS-mapping of (b).

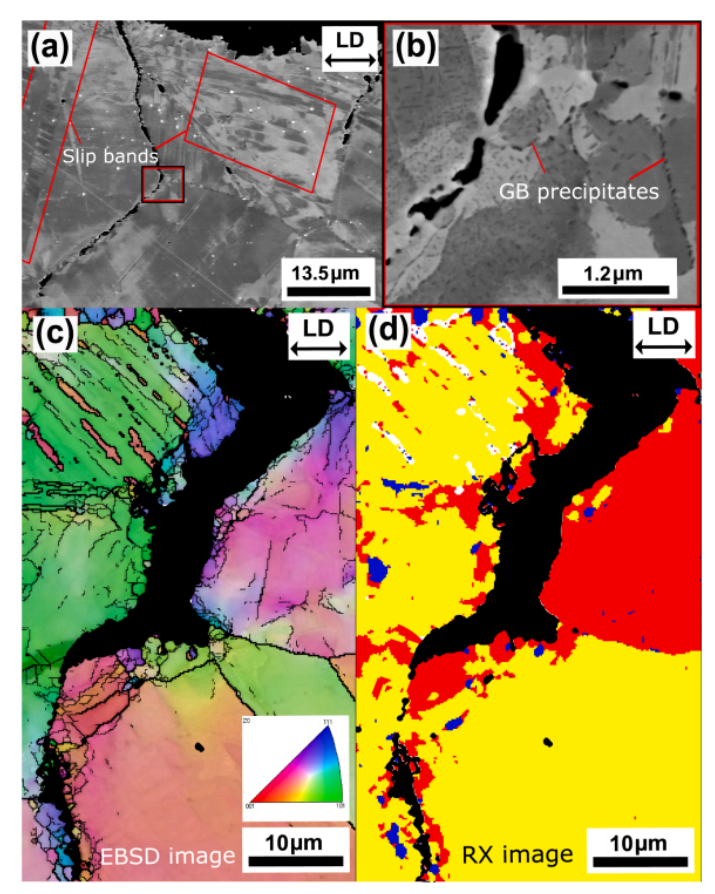


Figure 26: Crack overview at the specimen surface of Esshete 1250, t<sub>d</sub> = 600 s; (a) crack path overview, (b) zoomed in area in (a) and (c) EBSD-image of crack initiation close to the specimen surface, (d) recrystallized fraction analysis of (c).



In both cases, there are evidence of regions containing high density of planar slip bands (Figures 25 a and 26 a) which interact with the grain boundaries and the local residing precipitates, this can be seen in Figure 27 b and Figure 28 b.

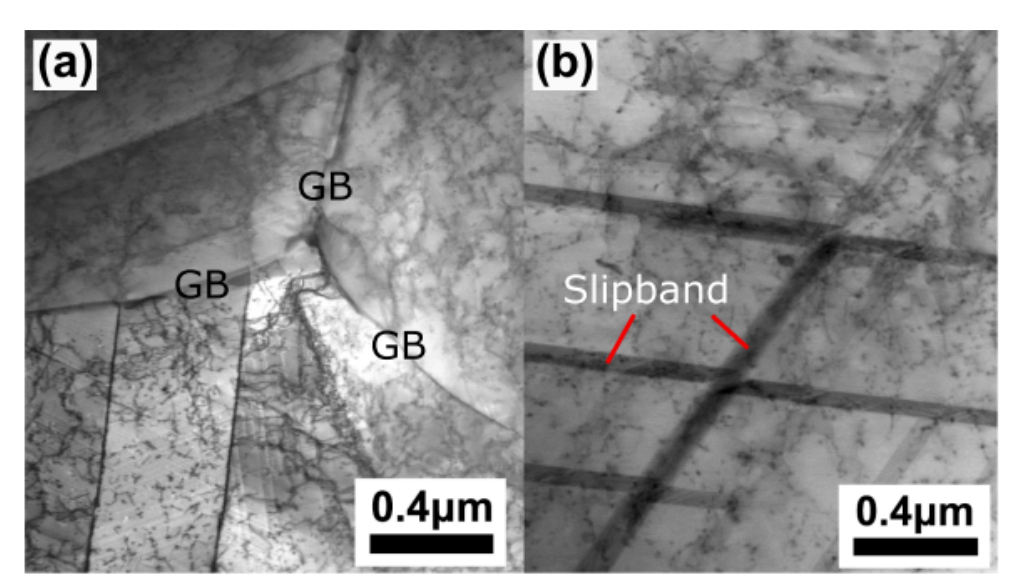


Figure 27: STEM bright field imaging of dislocation structure for Esshete 1250,  $t_d$  = 600 s; (a) at a grain boundary intersection, (b) in the interior of the grain.

According to the WDS analysis, presented in Figure 25 c and the STEM EDS-analysis, presented in Figure 28 b the precipitates in the grain boundaries and in the grain interiors would be Cr- and Nb-carbides. In Figure 28 a there are evidence of dislocation pinning Nb-carbide and holes originating from ground out precipitates.

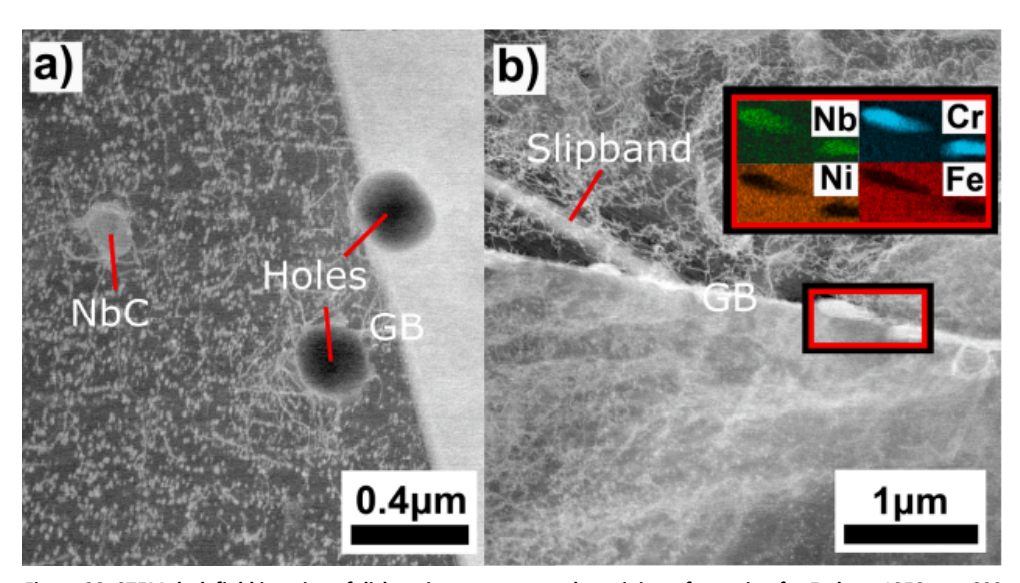


Figure 28: STEM dark field imaging of dislocation structure and precipitate formation for Esshete 1250, t<sub>d</sub> = 600 s; (a) Precipitates close to a grain boundary and the interaction with dislocations, (b) EDS-analysis of a precipitated grain boundary.

In contrast to the Sanicro 25 tests, formation of recrystallised grains in the crack tip plastic zone seems to be negligible, as indicated by Figure 26 d. For the tests with shortest dwell



time, t<sub>d</sub>=300 s, linkage of the fatigue-initiated cracks with the creep-initiated grain boundary cavities are less likely, but the same crack characteristics as for the longer t<sub>d</sub> tests is still observed according to the Sanicro 25 microstructure, as shown in the overview image Figure 29 a and the EBSD map of Figure 29 b. This contributes to overall reduced fatigue and creep damage. For Esshete 1250, the fatigue dominated damage contributes less to the overall damage of the precipitated grain boundaries.

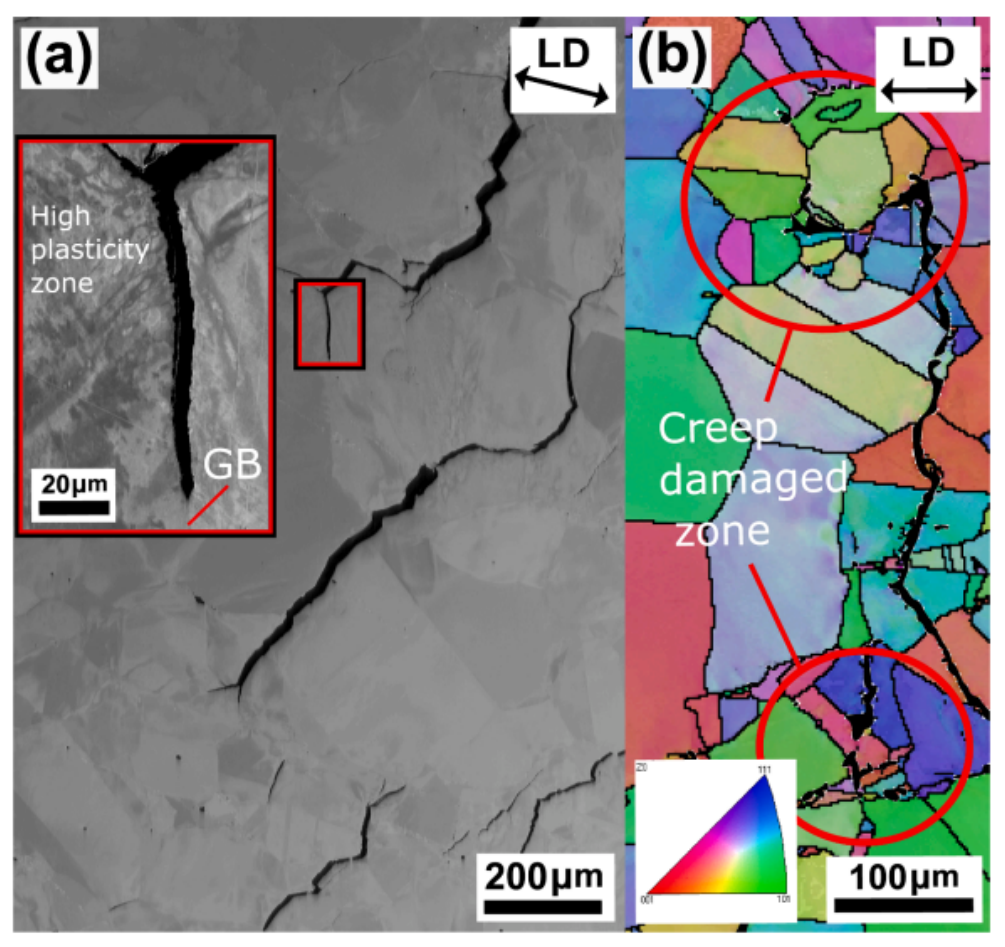


Figure 29: Sanicro 25 microstructure, td = 300 s; (a) crack propagation overview and zoomed in area of crack junction, (b) EBSD-image of crack propagation overview.

However, as shown in Figure 30 b, the crack path is still intergranular and similarly to the other Esshete 1250 tests this is because of the slip band interaction with the grain boundary precipitates, which is visible in the overview image Figure 30 a.

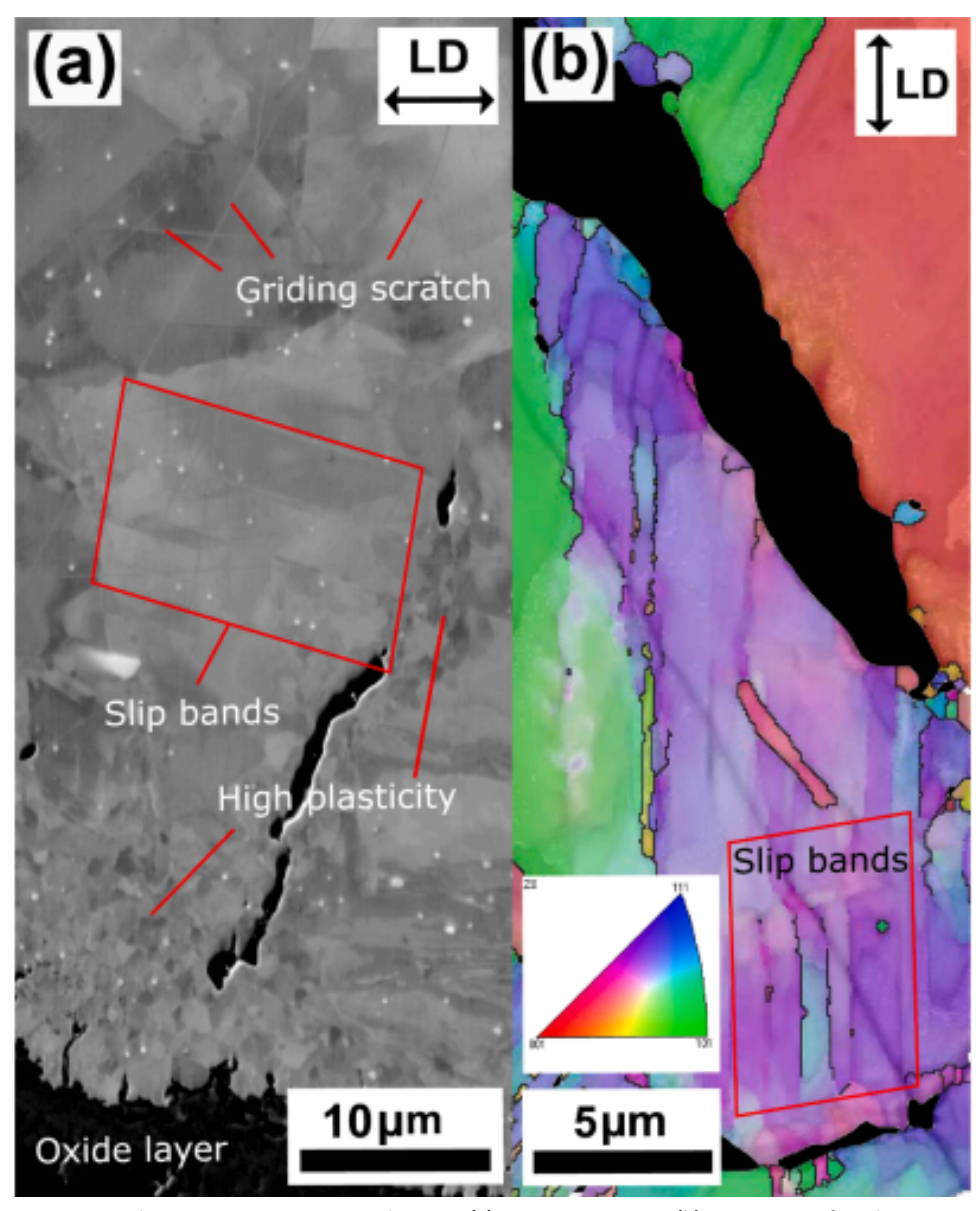


Figure 30: Esshete 1250 microstructure, td = 300 s; (a) initiation overview, (b) EBSD-image of crack initiation close to the specimen surface.

For Sanicro 25 a dynamic recrystallisation (DRX) process is present in the vicinity of the magnified crack tip during the high temperature fatigue and creep tests of Sanicro 25 (see Figure 22 a). The mechanism described for continuous DRX deemed the most reasonable to be involved during propagation of the crack and the interaction between the two damaging mechanisms, but to precisely define the process and its influence are hard without continuous examination of the crack propagation (interrupted testing) or high-resolution microscopy study of the crack tip. However, from current results, the crack propagation and interaction procedure are proposed in Figure 31: (1) A transgranular crack, originated form the surface by cracking of the oxide layer, form a plastic zone in the vicinity of the crack tip containing a region with high dislocation density. The dislocations rearrange and migrates into sub-networks to accommodate the high level of deformation (1–2). When a certain level of strain has been reached and the



misorientation of the low angle grain boundaries (LAGBs) is high enough, high angle grain boundaries (HAGB) and dislocation free recrystallized grains are created (3–4). Then during the dwell time, the development of diffusion-controlled creep damage of the grain boundaries is more effective (5). The crack now propagates along with high amount of branching and the preferred path is through the creep damaged recrystallized grain boundaries (5–6). The process of 1–6 (indicated by the arrow) is then repeated for the next propagation stage of the crack (7). If a nearby area contains pre-existing creep damage, the global transgranular propagating crack will interlink with this favourable crack path and thereby adding to the overall damage and accelerate the cyclic failure (7–8). In this way the crack propagation gains its interchanging, rough and jagged nature with unambiguous crack branching, as can be seen in Figure 21 a, Figure 22 a-c and Figure 29 a.

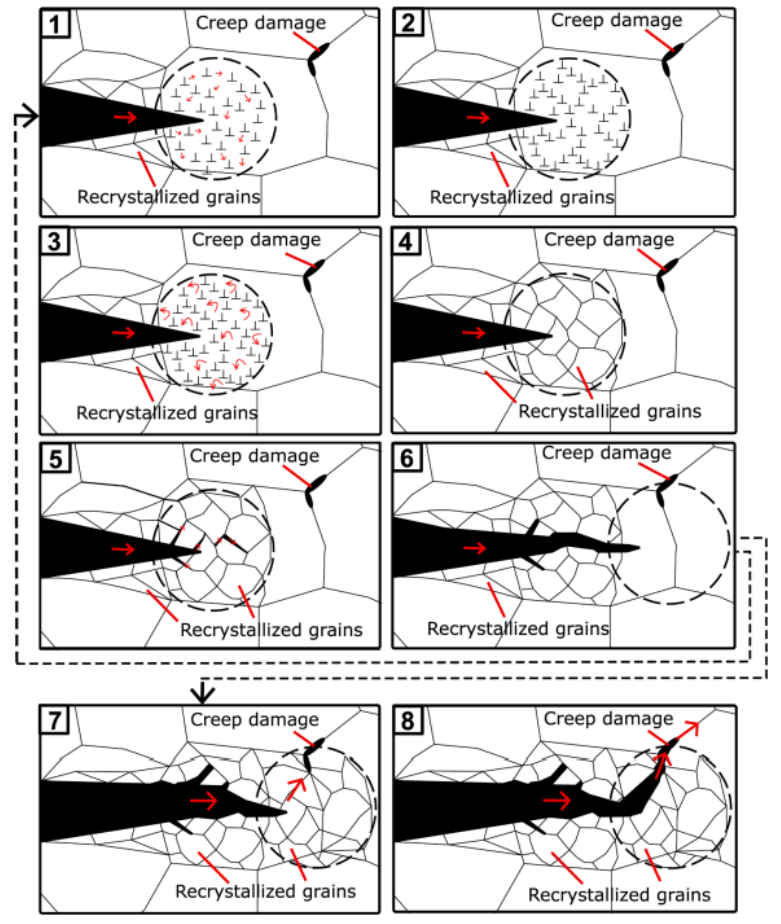


Figure 31: Schematic overview of the crack propagation and interaction process of Sanicro 25.

#### 3.3 INFLUENCE OF WELDING AND AGEING ON TOUGHNESS

During the project a suitable welding process have been investigated, however, the results was not good enough to proceed with within the project duration. Several combinations and parameters have been tried and much knowledge have been



gained droning the project. Since the results were not favorable they will not be presented in this report. Due to the limited time and budget the solution for this will be investigated at the companies besides this project.

#### 3.4 DESIGN FEASIBILITY STUDY

A design feasibility study was conducted and the results are summarized here. In this study one currently used boiler designs where final header material is P92 and compared it to Sanicro 25. It was shown that a benefit offered by Sanicro25 is the higher strength values that allows a thinner wall thickness to be used. In addition, some benefit could be obtained for boiler response time as well. However, response for bigger load changes are typically limited by durability of refractory linings.

# 3.5 CO-OPERATION, COMMUNICATION, DISSEMINATION AND REPORTING

The project has been a part of the industry initiative and forum KME, where an annual physical conference (except for during the pandemic) has been organized by KME via Energiforsk. The project has been presented at this conference each year.

In addition, eight publications in international recognized journals or conferences and one PhD thesis have been produced with the support from the project. These are listed in a section below. The conferences where the project has been presented are 22nd European Conference on Fracture (2018), EUROMAT 2019 (2019), 9th International Conference on Materials Structure and Micromechanics of Fracture (2019), 13th International Conference on the Mechanical Behaviour of Materials (2019) and 10th International Conference on Materials Structure and Micromechanics of Fracture (2022).



#### 4 Discussion

The thermomechanical fatigue performance of two candidate austenitic stainless steels were analysed [13, 16-20]. The influence of prolonged service degradation was simulated by pre-ageing of some specimens before TMF testing. The mechanical results were analysed and processed. Different microscopy techniques were used to investigate the microstructure after testing, to understand the mechanical behaviour of the alloys during TMF testing. In the project, both candidate materials experienced a detrimental effect on the TMF performance by the influence of pre-ageing. The reduction in TMF performance was attributed to an accelerated microstructural evolution that provided decreased effectiveness for impeding dislocation motion. Comparing TMF performance, Sanicro 25 showed compared to Esshete 1250 a better performance and higher strength for OP testing conditions including virgin and aged materials. This was attributed to the superior microstructural strengthening mechanisms during high temperature conditions. Consequently, the thermo-mechanical fatigue properties have been evaluated for the candidate materials tested in the project.

The mechanical response and microstructural evolution during high temperature fatigue and creep testing of the two austenitic stainless steels, Sanicro 25 and Esshete 1250, were investigated [13, 20, 21]. The two alloys exhibit different crack propagation and fatigue and creep behaviour, mainly due to the microstructural evolution during loading. Confirmation was found for the occurrence of coherent copper precipitates and incoherent Nb-carbides, which acted as dislocation obstacles and therefore add to the prominent hardening effect and high temperature properties of Sanicro 25 during the investigated fatigue and creep conditions. In addition, Z-phase particles located at the grain boundaries and larger Cr-carbides were also found. Nb-carbides were also found in the Esshete 1250 microstructure, which have the same effect as for Sanicro 25, but the grain boundaries contained sparsely placed Cr- and Nb-carbides which made them more susceptible to creep damage and intergranular crack propagation. Esshete 1250 solely experienced fracture along the grain boundaries, while the interior of the grains showed high plasticity in the form of pronounced fatigue induced slip bands. The interaction of the slip bands and the grain boundaries is considered to enhance the intergranular damage process. A fatigue and creep crack propagation process of Sanicro 25 was proposed, which involved dynamic recrystallization (DRX) of the crack tip plastic zone. This creates high angle grain boundaries that gives an energetically privileged path of the main crack, both during the fatigue and creep part of the test cycle, which adds to the overall reduction of cyclic life in an interactive manner. Thus, fatigue crack propagation behaviour and creep resistance have been evaluated for the candidate materials within the project.

Regarding the structural stability the precipitation behaviour of the candidate materials as well as their impact on the deformation, damage and failure mechanisms have been evaluated in the project [13, 17, 18, 21]. However, due to the unsatisfactory welding results the toughness of welded and aged materials could not be evaluated.



The project has showed that Sanicro 25 could be used to reduce the weight of the power plant components compared to currently used material and with maintained safety.

This project has resulted in new knowledge and understanding of the two candidate austenitic stainless steels mechanical and microstructural evolution during TMF, fatigue and creep as well as structural stability in regards of precipitation. This new knowledge can be used as a base for material selection regarding the future use of these materials in heavy section components in biomass-fired power plants. In addition, the new knowledge and understanding can be used for material development and to some extent lighter power plant design.

Hence the main industrial goal of verify the safety and reliability of heavy section Sanicro 25 to be used as new potential better material for headers and piping in biomass-fired power plants have to great extent been achieved. The main academic goals to produce one technical doctor as well as publication of articles on the new findings from the project have been achieved.



#### 5 Publication list

#### Journal papers

- H. Wärner, G. Chai, J. Moverare, M. Calmunger. High temperature fatigue of aged heavy section austenitic stainless steels, Materials, 2022, (15), 84.
- H. Wärner, J. Xu, G. Chai, J. Moverare, M. Calmunger. Microstructural evolution during high temperature dwell-fatigue of austenitic stainless steels, International Journal of Fatigue, 2021, (143), 105990.
- H. Wärner, M. Calmunger G. Chai, S. Johansson, J. Moverare. Thermomechanical fatigue behaviour of aged heat resistant austenitic alloys, International Journal of Fatigue, 2019, (127), pp. 509-521.

#### Conference papers

- M. Calmunger, H. Wärner, G. Chai, M. Segersäll. Thermomechanical Fatigue of Heat Resistant Austenitic Alloys, Structural Integrity Procedia, 2023, (43), pp. 130-135.
- H. Wärner, R. Eriksson, G. Chai, J. Moverare S. Johansson, M. Calmunger. Influence of ageing on thermomechanical fatigue of austenitic stainless steels, Procedia Structural Integrity, 2019, (23), pp. 354-359.
- M. Calmunger, H. Wärner, G. Chai, S. Johansson, J. Moverare. High temperature properties of austenitic stainless steels for future power plant applications, EUROMAT 2019, 2019.
- H. Wärner, M. Calmunger, G. Chai, S. Johansson, J. Moverare. Structural integrity and impact toughness of austenitic stainless steels, 13th International Conference on the Mechanical Behaviour of Materials (ICM13), 2019.
- H. Wärner, M. Calmunger, G. Chai, J. Polák, R. Petráš, M. Heczko, T. Kruml, S. Johansson, J. Moverare. Fracture and Damage Behavior in an Advanced Heat Resistant Austenitic Stainless Steel During LCF, TMF and CF, Structural Integrity Procedia, 2018, (13), pp. 843-848.

#### **Academic Theses**

H. Wärner. High Temperature Fatigue Behaviour of Austenitic Stainless Steel - Microstructural Evolution during Dwell-Fatigue and Thermomechanical Fatigue, 2021, PhD Thesis, ISBN 978-91-7929-666-7.



#### 6 References

- [1] Sadrul Islam, AKM, Ahiduzzaman, M. AIP Conference Proceedings 2012;1440:23.
- [2] Pettersson, J, Asteman, H, Svensson, J, Johansson, L. Oxidation of Metals 2005;64:23.
- [3] Margolin BZ, Shvetsova VA, Karzov GP. Int.J.Pressure Vessels Piping 1997;72:73.
- [4] Trygg L, Amiri S. Appl.Energy 2007;84:1319.
- [5] Yin J, Wu Z. Chin.J.Chem.Eng. 2009;17:849.
- [6] Viklund P, Hjörnhede A, Henderson P, Stålenheim A, Pettersson R. Fuel Process Technol 2013;105:106.
- [7] Reed RC. Superalloys: fundamentals and applications. Cambridge: Cambridge University Press, 2006.
- [8] Calmunger M. Final report (2018); KME 701.
- [9] Sourmail T. Materials Science and Technology 2001;17:1.
- [10] Calmunger M, Chai G, Johansson S, Moverare J. ICF13 2013
- [11] Christ H-. Materials Science and Engineering A 2007;468-470:98.
- [12] Moverare J. Final report (2014); KME 521.
- [13] H. Wärner. PhD Thesis (2021); ISBN 978-91-7929-666-7.
- [14] Calmunger, M, Chai, G, Johansson, S, Moverare, J. Theor. Appl. Mech. Lett. 2014, 4, 041004
- [15] Calmunger, M, Chai, C, Eriksson, R, Johansson, S, Moverare, J. Metall. Mater. Trans. A 2017, 48, 4525–4538
- [16] M. Calmunger, H. Wärner, G. Chai, M. Segersäll. Structural Integrity Procedia, 2023;43;130-135.
- [17] H. Wärner, G. Chai, J. Moverare, M. Calmunger. Materials, 2022;15;84.
- [18] H. Wärner, M. Calmunger G. Chai, S. Johansson, J. Moverare. International Journal of Fatigue, 2019;127;509-521.
- [19] H. Wärner, R. Eriksson, G. Chai, J. Moverare S. Johansson, M. Calmunger. Procedia Structural Integrity, 2019;23;354-359.
- [20] H. Wärner, M. Calmunger, G. Chai, J. Polák, R. Petráš, M. Heczko, T. Kruml, S. Johansson, J. Moverare. Structural Integrity Procedia, 2018;13;843-848
- [21] H. Wärner, J. Xu, G. Chai, J. Moverare, M. Calmunger. International Journal of Fatigue, 2021;143;105990.



# HEAVY SECTION AUSTENITIC STAINLESS STEEL FOR HEADERS AND PIPING IN HIGH-EFFICIENT BIOMASS-FIRED POWER PLANTS

This project has resulted in new knowledge and understanding of the two candidate austenitic stainless steels mechanical and microstructural evolution during TMF, fatigue and creep as well as structural stability in regards of precipitation. This new knowledge can be used as a base for material selection regarding the future use of these materials in heavy section components in biomass-fired power plants. In addition, the new knowledge and understanding can be used for material development and to some extent lighter power plant design

Vi gör energivärlden smartare!

Genom samarbete och dialog bedriver vi energiforskning så att ny kunskap skapar värde för näringsliv, kunder och samhället i stort. Vi är det naturliga navet i energiforskningen – en opartisk aktör till nytta för framtidens energisystem.

